FACULTY OF SCIENCES

Investigating the role of temperature-dependent *At*EH/Pan1 phosphorylation in *Arabidopsis thaliana*.

Dagmar De Jonckheere
Student number: 02309689

Promoter: Prof. Dr. ir. Daniël Van Damme

Scientific supervisor: Tingyu Zhu

Master's dissertation submitted to Ghent University to obtain the degree of Master of Science in Plant Biotechnology

Academic year: 2023 – 2024

UNIVERSITEIT GENT

Ghent University – Department of Plant Biotechnology and Bioinformatics
VIB – Center for Plant Systems Biology
Research Group: Advanced Live Cell Imaging

VIB-UGENT CENTER FOR PLANT SYSTEMS BIOLOGY

ABSTRACT

The plant plasma membrane (PM) serves as a vital lipid barrier containing integral proteins such as receptors and channels that facilitate interactions between the cell and its environment. Clathrin-mediated endocytosis (CME) is the predominant eukaryotic pathway for the selective internalisation of molecules, relying on the scaffolding protein clathrin. In plant CME, *Arabidopsis thaliana* EH/Pan1 proteins (*At*EH/Pan1) are critical subunits of the endocytic TPLATE complex. Recent studies of the warm temperature-regulated phosphoproteome have identified serine 900 of *At*EH1/Pan1 as being differentially phosphorylated under elevated temperature conditions. This finding suggests the existence of a temperature-dependent phosphorylation switch. Previous results from our lab showed that 35S:*At*EH1-GFP overexpression lines don't lift their leaves in response to a temperature of 28 °C, whereas wild-type Col-0 plants do. The project's objective was to investigate how altered protein phosphorylation of *At*EH1/Pan1 correlates with temperature-dependent plant developmental responses. To do this, I studied overexpression and mutant complementation in *Arabidopsis thaliana* using *At*EH1/Pan1 proteins with altered phosphorylation potential for ten distinct phosphorylation sites. My results showed that overexpression lines of phospho-dead and phospho-mimicking *At*EH1 isoforms abolished the 28 °C unresponsive phenotype seen in 35S:*At*EH1-GFP overexpression lines. This indicates a role for one or more of the ten different phosphorylation sites in the regulation of plant hyponasty. Since both phospho-dead and phospho-mimicking overexpression lines had the same phenotype, I concluded that phospho-mimicking doesn't necessarily have the same function as phosphorylation. In the second part of this research, I used a root growth assay at 21 °C and at 28 °C to show that the functionality of phospho-mutant *At*EH1 isoforms was not affected for root growth. I also showed that genotyping the complementation lines to assess the background of the *eh1-1* mutants using two PCR reactions is not ideal. I suggest that it is better to use other tests such as a viability stain with FDA or a Western blot targeting the native *At*EH1 protein with an anti-EH1 antibody.

INTRODUCTION

Plants, as sessile organisms, need to interact with and react to a changing environment to survive threats and to ensure reproduction. A key process in plant growth and

development is clathrin-mediated endocytosis (CME). On the other hand, there are reaction mechanisms such as leaf hyponasty to survive changes in temperature by providing a cooling mechanism.

CME controls cellular function.

CME is a conserved internalisation process throughout the eukaryotic kingdom. It plays a role in the internalisation of molecules such as hormone receptors and their associated ligands, protein channels etc. This process has been described in mammals, yeast, metazoans and plants. CME plays a role in several important physiological processes such as nutrient uptake, hormone transport and developmental regulation. Initiation, growth, vesicle budding, scission and uncoating are the different stages of CME. The TPLATE complex (TPC) is the earliest marker of CME, arriving at the site of vesicle formation before clathrin, the AP-2 adaptor complex and dynamin-related fission proteins (Gadeyne et al., 2014). TPC undergoes lipid-dependent nucleation by condensation at the plasma membrane and this plays an important role in clathrin recruitment and assembly from initiation to scission (Dragwidge et al., 2024). AP-2 arrives slightly later and will orchestrate vesicle coat formation by recruiting and linking clathrin to the endocytic cargo (Bashline et al., 2013). TPC plays a role in membrane curvature generation (Johnson et al., 2021). After the initiation and the growth phase, vesicle budding and scission are mediated by dynamin-related proteins 1 (DRP1) and DRP2. These proteins contain an N-terminal GTPase domain that is required for GTP hydrolysis to cleave the formed vesicles from the plasma membrane (Fujimoto et al., 2010; Johnson and Vert, 2017). The clathrin-coated vesicle moves through the plant cell guided by the actin cytoskeleton. The destination of the vesicles is the trans-Golgi network/early endosome (TGN/EE). Uncoating, the final step in CME, occurs gradually, just before or when the vesicle reaches the TGN/EE. The shed components are recycled for another round of endocytosis (Narasimhan et al., 2020).

The octameric TPLATE complex in plants and the hexameric TSET complex in the slime mold *Dictyostelium* share six components: TPLATE, TASH3, LOLITA, TML, TWD40-1, and TWD40-2. In addition, the TPLATE complex has two extra subunits in plants, *At*EH1/Pan1 and *At*EH2/Pan1 (Gadeyne et al., 2014; Yperman et al., 2021b). These *At*EH/Pan1 proteins show homology to the yeast proteins Pan1p and Ede1p due to the Eps15 homology (EH) domains at their N-terminus. The *At*EH/Pan1 proteins both contain

two EH domains that interact directly with anionic phospholipids such as phosphatidic acid and phosphatidylinositol 4,5-biphosphate (PIP_2). In addition to the EH domains, the *At*EH/Pan1 proteins contain a coiled-coil domain (Yperman et al., 2021b). This domain is likely involved in dimerisation (Gadeyne et al., 2014; Wang et al., 2019; Yperman et al., 2021a).

Previous studies have shown that endocytic mutants such as *tplate, tml-1*, *tml-2*, *ateh1-1*, *ateh2-1*, *twd40-1-1, twd40-2-1, tash3-2* have defects in pollen development (Gadeyne et al., 2014; Grones et al., 2022; Van Damme et al., 2006; Wang et al., 2019). These development defects result in male sterility. Plants carrying the defective genes shed shrivelled and normal pollen in a balanced ratio of 1:1. Insertion of a functional gene into these mutant lines rescues the phenotype. For example, endogenous expression of TML can rescue the male sterile phenotype of *tml-1* and *tml-2* mutants (Gadeyne et al., 2014).

Phosphoproteomic studies have shown differential phosphorylation of the *At*EH/Pan1 proteins at cold and high ambient temperatures of 2 °C and 27 °C (Tan et al., 2021; Vu et al., 2021). Seedlings of the ecotype Col-0 were sampled at 21 °C, the control temperature, and during incubation at 27 °C, the high ambient temperature. Serine 900 (S900) of *At*EH/Pan1 was shown to be hyper phosphorylated at 27 °C (Vu et al., 2021). Phosphorylation of the protein can lead to a conformational change in the structure. The conformational change could have multiple functions: direct temperature sensing, change in protein localisation, causing different interactions with other biomolecules, protein misfolding or as a signal for quality control (Vu et al., 2019a).

Plants respond to a warming world via thermomorphogenesis.

Changes in protein conformation take place at the cellular level. At the macroscopic level, plants respond to temperature through thermomorphogenesis, a nastic movement in response to the indirect cue of temperature. Examples include hypocotyl elongation, inhibition of seed germination, flowering, root elongation, fruit dehiscence and leaf thermonasty. These nastic movements are regulated by different molecular mechanisms (Vu et al., 2019b). Here, I will discuss leaf thermonasty, which is the upward bending of leaves in response to high ambient temperatures, also known as hyponasty. This allows the plant to lower its leaf temperature. This was shown in a simple experiment in which the leaf temperature of Col-0 plants and a hyponasty-defective mutant such as *pif4-101*

were compared. The experiment showed a difference in temperature between the lifted leaves of Col-0 and the non-lifted leaves of *pif4-101*. The lifted leaves of Col-0 were cooler than those of *pif4-101.* When the leaves of *pif4-101* were artificially lifted, the temperature of the leaves was similar to that of the leaves of Col-0. Hyponasty is therefore a mechanism by which the plants cool down. Leaf thermonasty was impaired in plants overexpressing a constitutive form of phyB, suggesting that the phyB-mediated temperature sensing mechanism and leaf thermonasty are functionally linked (Kim et al., 2019). The molecular mechanisms of hyponasty have been partly elucidated. Leaf movement is based on the synthesis and redistribution of auxin, which accumulates on the abaxial side of the leaf and causes asymmetric petiole growth. In line with the role of auxin in this process, *yuc8* and *pin3-4* mutants, of which the former plays a role in auxin biosynthesis, and the latter in mediating polar auxin transport, are also defective in thermonasty (Park et al., 2019).

The phosphorylation of *At*EH1 links the response to temperature changes with endocytosis.

Observations in our laboratory have shown that *At*EH1/Pan1 was differentially phosphorylated at several serine residues in the C-terminal end at different temperatures. Other experiments have shown that *At*EH1/Pan1 overexpression lines responded differently to high ambient temperatures than Col-0. While Col-0 plants lifted their leaves in response to a temperature of 28 °C for 6 hours, the *At*EH1 overexpression lines failed to do so. Based on these two independent observations, I formulated my hypothesis and an additional research question. I hypothesised that there is a link between temperature-dependent phosphorylation of *At*EH1 and thermonasty. *At*EH1/Pan1 phospho-dead and phospho-mimicking overexpression lines at ten distinct residues were used to test this hypothesis. I didn't know if these phospho-mutations affected the functionality of *At*EH1/Pan1 at room temperature or at a temperature of 28 °C. Therefore, I tested this by expressing the same mutant genes under the expression of the endogenous promoter p*At*EH1 in *eh1-1*(+/-) mutants. These mutants fail to generate homozygous mutant offspring due to the male sterile phenotype, the insertion of a functional protein in these mutants results in homozygous *eh1-1*(-/-) plants by complementing the male sterility phenotype.

RESULTS

In the first part of the results, I searched for a connection between endocytosis and temperature-mediated hyponasty. In this part, I selected and used overexpression lines of *At*EH1 phospho-mutants. In the second part, *eh1-1*(+/-) mutants were complemented with the *At*EH1 phospho-mutants, to explore the functionality of the mutations at high ambient temperatures.

Differential phosphorylation of *At*EH1/Pan1 plays a role in temperature-dependent plant morphogenesis.

To test whether differential phosphorylation plays a role in thermomorphogenesis, I used *Arabidopsis* overexpression lines of *AtEH1* encoding phospho-dead and phospho-mimicking isoforms. These protein isoforms contain alanine residues or aspartic acid residues instead of serine residues at ten positions in the C-terminal tail, termed 10SA and 10SD, respectively. These lines I worked with were selected for a single locus transformation events in the homozygous state throughout the T2 and T3 generation. This is particularly important for consistency and reproducibility of future results. In addition, it is easier to characterise the effects of a mutant gene when it is present at a single locus than when it is present at multiple loci. I wanted to select homozygous lines to ensure a consistent level of expression in the line and its offspring.

Selection of plants carrying the construct of interest at a single locus.

I was interested in plant lines carrying the gene of interest at a single locus. I used the T2 generation of the overexpression lines to find single locus events. Since the Mendelian segregation law states that a trait defined by a single gene will segregate in a 3:1 ratio, a single locus event is also characterised by this ratio (Table 1 and Table 2). The seedlings sensitive to Basta were small and pale yellow while those resistant to Basta were large and green. I did a χ^2 test to see which lines do not segregate 3:1. I selected the lines with a χ^2-value smaller than one and a GFP signal visible in observations with a stereomicroscope. For the phospho-dead variants of *At*EH1, I tested eleven lines and selected two lines that met both selection criteria (Table 1). For the phospho-mimicking mutants of *At*EH1, I tested 28 lines and selected ten lines that met both criteria (Table 2). Sixteen to twenty plants of the selected lines were grown in soil for self-pollination to produce seed for the T3 generation.

Selection of plants carrying the construct of interest in a homozygous state at a single genetic locus.

In the T3 generation, I was interested in the lines in which the construct was present in both alleles. I sowed eight lines per T2 parent line to test for homozygosity. The lines in which all seedlings were resistant to Basta are homozygous (Table 3 and Table 4) and were selected for expression analysis. For the phospho-dead *At*EH1 isoforms, I selected five lines for expression analysis (Table 3). For the phospho-mimicking *At*EH1 isoforms, I selected 34 lines for expression analysis (Table 4).

Table 1 List of all T2 phospho-dead overexpression lines tested for a 3:1 segregation ratio. For each line, the number of Basta sensitive, Basta resistant and total amount of seedlings counted are given. These values were used to calculate the χ^2. Lines with a χ^2 value < 1 and a visible GFP signal were selected to produce the next generation (T3). The selected lines are underlined.

Order	Unique identifier	Construct	Basta sensitive	Basta resistant	Total amount of seedlings	χ^2	GFP signal
L1	S12476	35S:*At*EH1-10SA-GSL-mGFP(B)	11	34	45	0.01	Moderate
L2	S12477	35S:*At*EH1-10SA-GSL-mGFP(B)	3	36	39	6.23	
L3	S12478	35S:*At*EH1-10SA-GSL-mGFP(B)	14	22	36	3.70	
L4	S12479	35S:*At*EH1-10SA-GSL-mGFP(B)	18	33	51	2.88	
L5	S12480	35S:*At*EH1-10SA-GSL-mGFP(B)	2	46	48	11.11	
L6	S12481	35S:*At*EH1-10SA-GSL-mGFP(B)	9	28	37	0.01	Absent
L7	S12482	35S:*At*EH1-10SA-GSL-mGFP(B)	5	46	51	6.28	
L8	S12483	35S:*At*EH1-10SA-GSL-mGFP(B)	2	48	50	11.76	
L9	S12484	35S:*At*EH1-10SA-GSL-mGFP(B)	11	37	48	0.11	Strong
L10	S12485	35S:*At*EH1-10SA-GSL-mGFP(B)	20	31	51	5.50	
L11	S12486	35S:*At*EH1-10SA-GSL-mGFP(B)	18	33	51	2.88	

Table 2 List of all T2 phospho-mimicking overexpression lines tested for a 3:1 segregation ratio. For each line, the number of Basta sensitive, Basta resistant and total amount of seedlings counted are given. These values are used to calculate the χ^2. Lines with a χ^2 value < 1 and a visible GFP signal are selected to produce the next generation (T3). The selected lines are underlined.

Order	Unique identifier	Construct	Basta sensitive	Basta resistant	Total amount of seedlings	χ^2	GFP signal
L1	S12487	35S:*At*EH1-10SD-GSL-mGFP(B)	15	36	51	0.53	Strong
L2	S12488	35S:*At*EH1-10SD-GSL-mGFP(B)	9	42	51	1.47	
L3	S12489	35S:*At*EH1-10SD-GSL-mGFP(B)	1	50	51	14.44	
L4	S12490	35S:*At*EH1-10SD-GSL-mGFP(B)	3	48	51	9.94	
L5	S12491	35S:*At*EH1-10SD-GSL-mGFP(B)	17	32	49	2.46	
L6	S12492	35S:*At*EH1-10SD-GSL-mGFP(B)	6	33	39	1.92	
L7	S12493	35S:*At*EH1-10SD-GSL-mGFP(B)	7	44	51	3.46	
L8	S12494	35S:*At*EH1-10SD-GSL-mGFP(B)	3	47	50	9.63	
L9	S12495	35S:*At*EH1-10SD-GSL-mGFP(B)	19	32	51	4.08	
L10	S12496	35S:*At*EH1-10SD-GSL-mGFP(B)	3	48	51	9.94	
L11	S12497	35S:*At*EH1-10SD-GSL-mGFP(B)	16	35	51	1.10	
L12	S12498	35S:*At*EH1-10SD-GSL-mGFP(B)	4	44	48	7.11	
L13	S12499	35S:*At*EH1-10SD-GSL-mGFP(B)	4	47	51	8.01	
L14	S12500	35S:*At*EH1-10SD-GSL-mGFP(B)	12	30	42	0.29	Moderate

Order	Unique identifier	Construct	Basta sensitive	Basta resistant	Total amount of seedlings	χ^2	GFP signal
L15	S12501	35S:*At*EH1-10SD-GSL-mGFP(B)	11	40	51	0.32	Moderate
L16	S12502	35S:*At*EH1-10SD-GSL-mGFP(B)	5	46	51	6.28	
L17	S12503	35S:*At*EH1-10SD-GSL-mGFP(B)	11	37	48	0.11	Moderate
L18	S12504	35S:*At*EH1-10SD-GSL-mGFP(B)	3	18	21	1.29	
L19	S12505	35S:*At*EH1-10SD-GSL-mGFP(B)	15	36	51	0.53	Moderate
L20	S12506	35S:*At*EH1-10SD-GSL-mGFP(B)	11	40	51	0.32	Moderate
L21	S12507	35S:*At*EH1-10SD-GSL-mGFP(B)	5	46	51	6.28	
L22	S12508	35S:*At*EH1-10SD-GSL-mGFP(B)	13	28	41	0.98	Weak
L23	S12509	35S:*At*EH1-10SD-GSL-mGFP(B)	8	44	52	2.56	
L24	S12510	35S:*At*EH1-10SD-GSL-mGFP(B)	7	27	34	0.35	Moderate
L25	S12511	35S:*At*EH1-10SD-GSL-mGFP(B)	11	27	38	0.32	Strong
L26	S12512	35S:*At*EH1-10SD-GSL-mGFP(B)	10	41	51	0.79	Moderate
L27	S12513	35S:*At*EH1-10SD-GSL-mGFP(B)	2	49	51	12.08	
L28	S12514	35S:*At*EH1-10SD-GSL-mGFP(B)	1	104	105	32.38	

Table 3 List of T3 phospho-dead overexpression lines tested for homozygosity of the gene of interest. I tested 8 plants for each T2 parent line. If at least one seedling was sensitive, the line was classified as heterozygous. The unique identifier of the parent line is included to track down independent lines. The selected lines are underlined.

Order	Unique identifier	Construct	Homozygous for Basta resistance	Unique identifier parent line (T2)
L1.1	S13659	35S:*At*EH1-10SA-GSL-mGFP(B)	Yes	S12476
L1.2	S13660	35S:*At*EH1-10SA-GSL-mGFP(B)	No	S12476
L1.3	S13661	35S:*At*EH1-10SA-GSL-mGFP(B)	Yes	S12476
L1.4	S13662	35S:*At*EH1-10SA-GSL-mGFP(B)	No	S12476
L1.5	S13663	35S:*At*EH1-10SA-GSL-mGFP(B)	No	S12476
L1.6	S13664	35S:*At*EH1-10SA-GSL-mGFP(B)	Yes	S12476
L1.7	S13665	35S:*At*EH1-10SA-GSL-mGFP(B)	No	S12476
L1.8	S13666	35S:*At*EH1-10SA-GSL-mGFP(B)	No	S12476
L9.1	S13848	35S:*At*EH1-10SA-GSL-mGFP(B)	No	S12484
L9.2	S13849	35S:*At*EH1-10SA-GSL-mGFP(B)	Yes	S12484
L9.3	S13850	35S:*At*EH1-10SA-GSL-mGFP(B)	No	S12484
L9.4	S13851	35S:*At*EH1-10SA-GSL-mGFP(B)	Yes	S12484
L9.5	S13852	35S:*At*EH1-10SA-GSL-mGFP(B)	No	S12484
L9.6	S13853	35S:*At*EH1-10SA-GSL-mGFP(B)	No	S12484

Order	Unique identifier	Construct	Homozygous for Basta resistance	Unique identifier parent line (T2)
L9.7	S13854	35S:*At*EH1-10SA-GSL-mGFP(B)	No	S12484
L9.8	S13855	35S:*At*EH1-10SA-GSL-mGFP(B)	No	S12484

Table 4 List of T3 phospho-mimicking overexpression lines tested for homozygosity of the gene of interest. I tested 8 plants for each T2 parent line. If at least one seedling was sensitive, the line was classified as heterozygous. The unique identifier of the parent line is included to track down independent lines. The selected lines are underlined.

Order	Unique identifier	Construct	Homozygous for Basta resistance	Unique identifier parent line (T2)
L6.1	S13695	35S:*At*EH1-10SD-GSL-mGFP(B)	Yes	S12492
L6.2	S13696	35S:*At*EH1-10SD-GSL-mGFP(B)	Yes	S12492
L6.3	S13697	35S:*At*EH1-10SD-GSL-mGFP(B)	No	S12492
L6.4	S13698	35S:*At*EH1-10SD-GSL-mGFP(B)	No	S12492
L6.5	S13699	35S:*At*EH1-10SD-GSL-mGFP(B)	Yes	S12492
L6.6	S13700	35S:*At*EH1-10SD-GSL-mGFP(B)	Yes	S12492
L6.7	S13701	35S:*At*EH1-10SD-GSL-mGFP(B)	No	S12492
L6.8	S13702	35S:*At*EH1-10SD-GSL-mGFP(B)	No	S12492
L18.1	S13716	35S:*At*EH1-10SD-GSL-mGFP(B)	Yes	S12504
L18.2	S13717	35S:*At*EH1-10SD-GSL-mGFP(B)	No	S12504

Order	Unique identifier	Construct	Homozygous for Basta resistance	Unique identifier parent line (T2)
L18.3	S13718	35S:*At*EH1-10SD-GSL-mGFP(B)	No	S12504
L18.4	S13719	35S:*At*EH1-10SD-GSL-mGFP(B)	No	S12504
L18.5	S13720	35S:*At*EH1-10SD-GSL-mGFP(B)	Yes	S12504
L18.6	S13721	35S:*At*EH1-10SD-GSL-mGFP(B)	Yes	S12504
L18.7	S13722	35S:*At*EH1-10SD-GSL-mGFP(B)	No	S12504
L18.8	S13723	35S:*At*EH1-10SD-GSL-mGFP(B)	No	S12504
L24.1	S13725	35S:*At*EH1-10SD-GSL-mGFP(B)	Yes	S12510
L24.2	S13726	35S:*At*EH1-10SD-GSL-mGFP(B)	No	S12510
L24.3	S13727	35S:*At*EH1-10SD-GSL-mGFP(B)	No	S12510
L24.4	S13728	35S:*At*EH1-10SD-GSL-mGFP(B)	Yes	S12510
L24.5	S13729	35S:*At*EH1-10SD-GSL-mGFP(B)	Yes	S12510
L24.6	S13730	35S:*At*EH1-10SD-GSL-mGFP(B)	No	S12510
L24.7	S13731	35S:*At*EH1-10SD-GSL-mGFP(B)	No	S12510
L24.8	S13732	35S:*At*EH1-10SD-GSL-mGFP(B)	No	S12510
L1.1	S13907	35S:*At*EH1-10SD-GSL-mGFP(B)	No	S12487
L1.2	S13908	35S:*At*EH1-10SD-GSL-mGFP(B)	No	S12487

Order	Unique identifier	Construct	Homozygous for Basta resistance	Unique identifier parent line (T2)
L1.3	S13909	35S:*At*EH1-10SD-GSL-mGFP(B)	No	S12487
L1.4	S13910	35S:*At*EH1-10SD-GSL-mGFP(B)	No	S12487
L1.5	S13911	35S:*At*EH1-10SD-GSL-mGFP(B)	Yes	S12487
L1.6	S13912	35S:*At*EH1-10SD-GSL-mGFP(B)	Yes	S12487
L1.7	S13913	35S:*At*EH1-10SD-GSL-mGFP(B)	Yes	S12487
L1.8	S13914	35S:*At*EH1-10SD-GSL-mGFP(B)	Yes	S12487
L15.1	S13945	35S:*At*EH1-10SD-GSL-mGFP(B)	No	S12501
L15.2	S13946	35S:*At*EH1-10SD-GSL-mGFP(B)	Yes	S12501
L15.3	S13947	35S:*At*EH1-10SD-GSL-mGFP(B)	Yes	S12501
L15.4	S13948	35S:*At*EH1-10SD-GSL-mGFP(B)	No	S12501
L15.5	S13949	35S:*At*EH1-10SD-GSL-mGFP(B)	No	S12501
L15.6	S13950	35S:*At*EH1-10SD-GSL-mGFP(B)	No	S12501
L15.7	S13951	35S:*At*EH1-10SD-GSL-mGFP(B)	No	S12501
L15.8	S13952	35S:*At*EH1-10SD-GSL-mGFP(B)	No	S12501
L17.1	S13965	35S:*At*EH1-10SD-GSL-mGFP(B)	No	S12503
L17.2	S13966	35S:*At*EH1-10SD-GSL-mGFP(B)	No	S12503

Order	Unique identifier	Construct	Homozygous for Basta resistance	Unique identifier parent line (T2)
L17.3	S13967	35S:*At*EH1-10SD-GSL-mGFP(B)	Yes	S12503
L17.4	S13968	35S:*At*EH1-10SD-GSL-mGFP(B)	No	S12503
L17.5	S13969	35S:*At*EH1-10SD-GSL-mGFP(B)	Yes	S12503
L17.6	S13970	35S:*At*EH1-10SD-GSL-mGFP(B)	Yes	S12503
L17.7	S13971	35S:*At*EH1-10SD-GSL-mGFP(B)	Yes	S12503
L17.8	S13972	35S:*At*EH1-10SD-GSL-mGFP(B)	Yes	S12503
L19.1	S13995	35S:*At*EH1-10SD-GSL-mGFP(B)	No	S12505
L19.2	S13996	35S:*At*EH1-10SD-GSL-mGFP(B)	No	S12505
L19.3	S13997	35S:*At*EH1-10SD-GSL-mGFP(B)	No	S12505
L19.4	S13998	35S:*At*EH1-10SD-GSL-mGFP(B)	Yes	S12505
L19.5	S13999	35S:*At*EH1-10SD-GSL-mGFP(B)	No	S12505
L19.6	S14000	35S:*At*EH1-10SD-GSL-mGFP(B)	Yes	S12505
L19.7	S14001	35S:*At*EH1-10SD-GSL-mGFP(B)	No	S12505
L19.8	S14002	35S:*At*EH1-10SD-GSL-mGFP(B)	Yes	S12505
L20.1	S14015	35S:*At*EH1-10SD-GSL-mGFP(B)	Yes	S12506
L20.2	S14016	35S:*At*EH1-10SD-GSL-mGFP(B)	No	S12506

Order	Unique identifier	Construct	Homozygous for Basta resistance	Unique identifier parent line (T2)
L20.3	S14017	35S:*At*EH1-10SD-GSL-mGFP(B)	No	S12506
L20.4	S14018	35S:*At*EH1-10SD-GSL-mGFP(B)	No	S12506
L20.5	S14019	35S:*At*EH1-10SD-GSL-mGFP(B)	No	S12506
L20.6	S14020	35S:*At*EH1-10SD-GSL-mGFP(B)	No	S12506
L20.7	S14021	35S:*At*EH1-10SD-GSL-mGFP(B)	Yes	S12506
L20.8	S14022	35S:*At*EH1-10SD-GSL-mGFP(B)	Yes	S12506
L25.1	S14047	35S:*At*EH1-10SD-GSL-mGFP(B)	No	S12511
L25.2	S14048	35S:*At*EH1-10SD-GSL-mGFP(B)	No	S12511
L25.3	S14049	35S:*At*EH1-10SD-GSL-mGFP(B)	Yes	S12511
L25.4	S14050	35S:*At*EH1-10SD-GSL-mGFP(B)	No	S12511
L25.5	S14051	35S:*At*EH1-10SD-GSL-mGFP(B)	Yes	S12511
L25.6	S14052	35S:*At*EH1-10SD-GSL-mGFP(B)	No	S12511
L25.7	S14053	35S:*At*EH1-10SD-GSL-mGFP(B)	No	S12511
L25.8	S14054	35S:*At*EH1-10SD-GSL-mGFP(B)	No	S12511
L26.1	S14067	35S:*At*EH1-10SD-GSL-mGFP(B)	Yes	S12512
L26.2	S14068	35S:*At*EH1-10SD-GSL-mGFP(B)	Yes	S12512

Order	Unique identifier	Construct	Homozygous for Basta resistance	Unique identifier parent line (T2)
L26.3	S14069	35S:*At*EH1-10SD-GSL-mGFP(B)	Yes	S12512
L26.4	S14070	35S:*At*EH1-10SD-GSL-mGFP(B)	No	S12512
L26.5	S14071	35S:*At*EH1-10SD-GSL-mGFP(B)	Yes	S12512
L26.6	S14072	35S:*At*EH1-10SD-GSL-mGFP(B)	Yes	S12512
L26.7	S14073	35S:*At*EH1-10SD-GSL-mGFP(B)	No	S12512
L26.8	S14074	35S:*At*EH1-10SD-GSL-mGFP(B)	No	S12512

Differential phosphorylation of *At*EH1/Pan1 is related to temperature-dependent plant morphogenesis.

To examine the phenotypic effects of the mutant lines, I first wanted to know the expression level of the mutant *At*EH1 protein of each individual line. This knowledge is important to allow me to discriminate between results obtained due to the effects of the construct and results obtained due to the effects of the expression level. Therefore, I carried out a Western blot to check protein levels. The images of the gels and blots were used to quantify the protein levels for each line relative to the protein levels of the control line 35S*:At*EH1-GFP (Figure 1 and Supplemental Figure 1). Based on these results, I selected lines with different expression levels. For the phospho-dead mutant lines, there were only two independent overexpression lines available, thus I selected these. For the phospho-dead mutant lines, multiple independent lines were available, and I decided to choose four, each with a different expression level. For both mutations, I included one line with a higher expression level than the expression level of the control line 35S:*At*EH1-GFP, the other lines had expression levels that were lower than those of the control line 35S:*At*EH1-GFP.

Previously in our lab, it was found that lines overexpressing AtEH1 (35S:AtEH1-GFP) had a different phenotype from wild-type (Col-0) lines when incubated at 28 °C for 6 hours. The wild-type plants bend their leaves upwards at 28 °C, whereas the 35S:AtEH1-GFP lines don't respond to this high ambient temperature. I wanted to test how the overexpression lines of the mutant AtEH1 gene respond to this high ambient temperature. To examine this, I included Col-0 and 35S:AtEH1-GFP as control lines. Images were taken before incubation (0h, 21 °C) and after 6 hours of incubation at 28 °C (6h, 28 °C) for quantification (Figure 2B). The hyponasty test was quantified by measuring the difference in height of the highest leaf (Figure 2A). A Tukey post-hoc test showed a significant difference between the 35S:AtEH1-GFP control line and the phospho-mutant overexpression lines. These phospho-mutant overexpression lines showed no significant differences with the Col-0 control line (Figure 2C). Based on these results, I formulated two hypotheses. The first hypothesis is that the 35S:AtEH1-GFP used as a control in this experiment has a different phenotype at high ambient

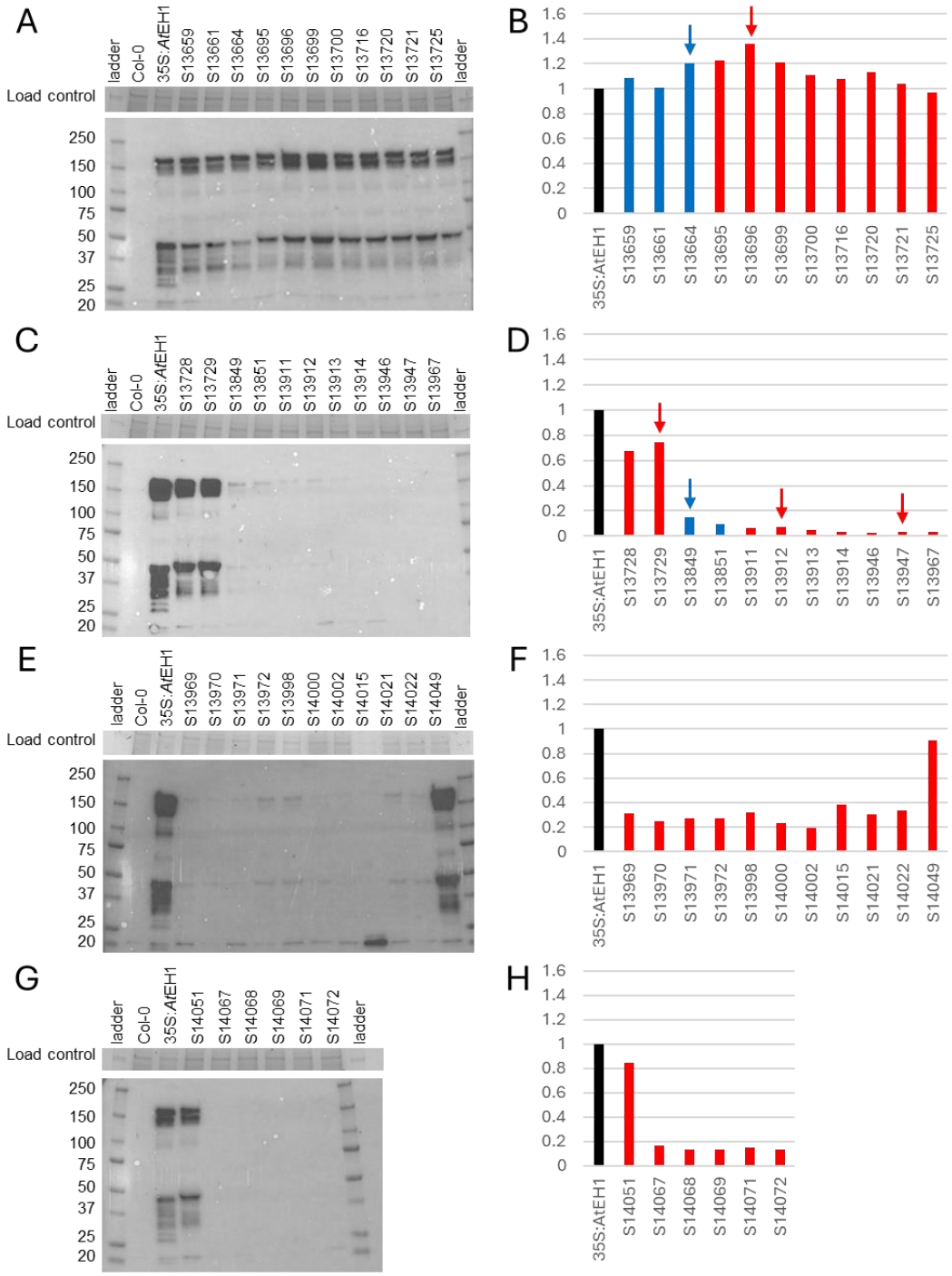

Figure 1 Western blot with anti-GFP antibody to visualise the overexpressed AtEH1 proteins (A, C, E, G) and quantification of the expression levels for each individual line and normalised to the 35S:AtEH1-GFP control line (B, D, F, H). LC = in stain loading control, 35S:AtEH1-GFP control lines are black, 10SA lines are blue, 10SD lines are red, selected lines are marked with an arrow.

temperatures due to overexpression of AtEH1. My second hypothesis is that the phospho-mimicking is not acting the same as an actual phosphorylation, causing both

phospho-mutants to have the same phenotype. Under this hypothesis, the causal phosphorylated residue is one of the ten tested residues, since the overexpression of *At*EH1 isoforms containing the mutated residues abolishes the overexpression phenotype of *At*EH1.

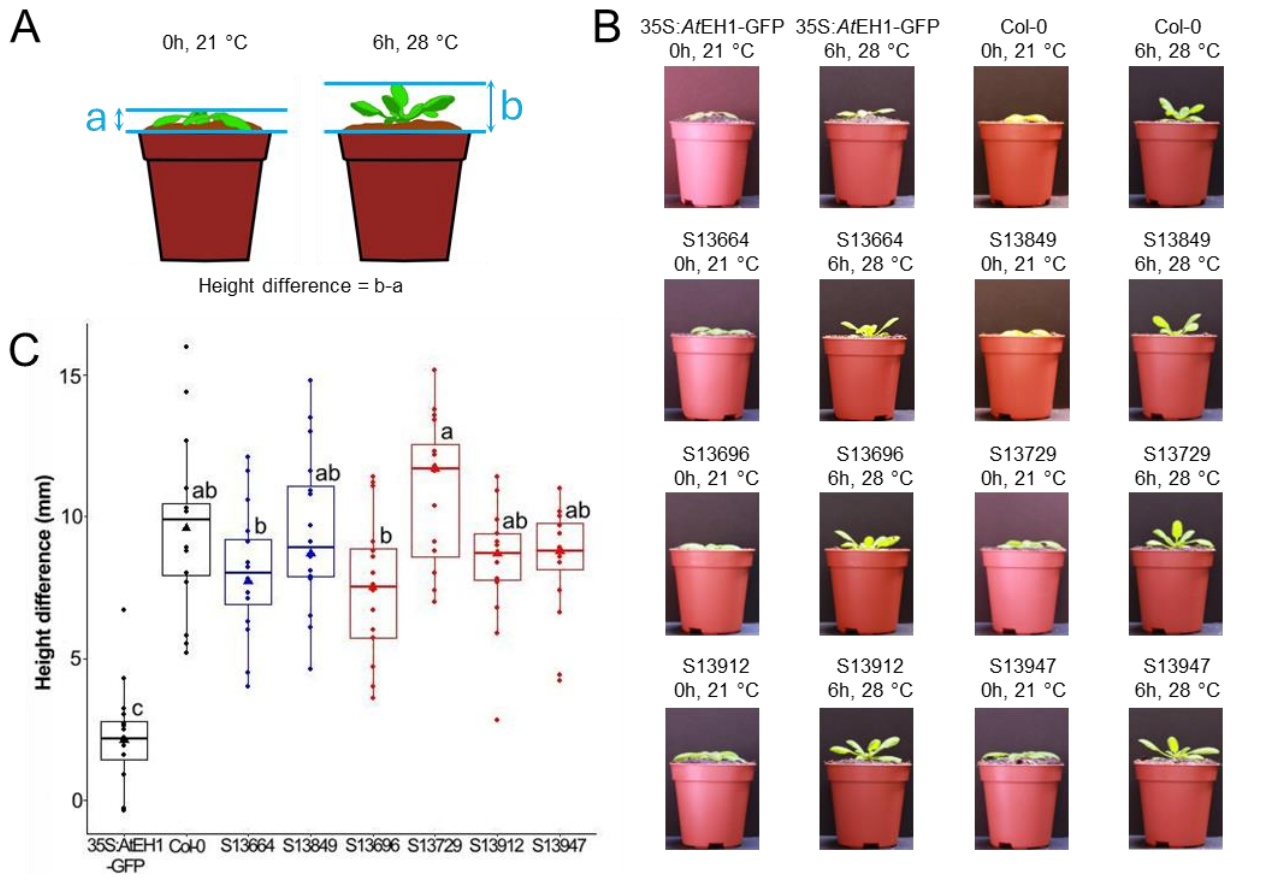

Figure 2 Leaf hyponasty assay of the phospho-mutated isoform overexpression lines. Diagram of a plant at 0h and 6h which is showing how this assay is quantified. At 6h, the distance between the highest leaf and the top of the pot is measured. At 0h the distance between the same leaf and the top of the pot is measured. The height difference is calculated based on these measurements (A). Representative images of all lines included in this test (B). Quantification of the leaf hyponasty test. 16 plants were tested for each line. The triangle indicated on the box plots corresponds to the images in B. Groups with different letters are significantly different from each other ($p < 0.05$), according to a post-hoc Tukey test. The whiskers show the minimum and maximum values while the box represents the first quantile (25 %), the median and the third quantile (75 %)(C).

The first hypothesis was tested using three independent 35S:*At*EH1-GFP lines, including the control line from the previous experiment (35S:*At*EH1-GFPa). All three control lines have a similar expression level and a similar phenotype (Figure 3A,B and Supplemental Figure 2). The hyponasty test showed significant differences between the Col-0 and p*At*EH1:*At*EH1-GFP control lines and the three 35S:*At*EH1-GFP lines (Figure 3D).

I conclude that the phenotype of the overexpression line of *At*EH1 is not caused by the insertion site of the construct.

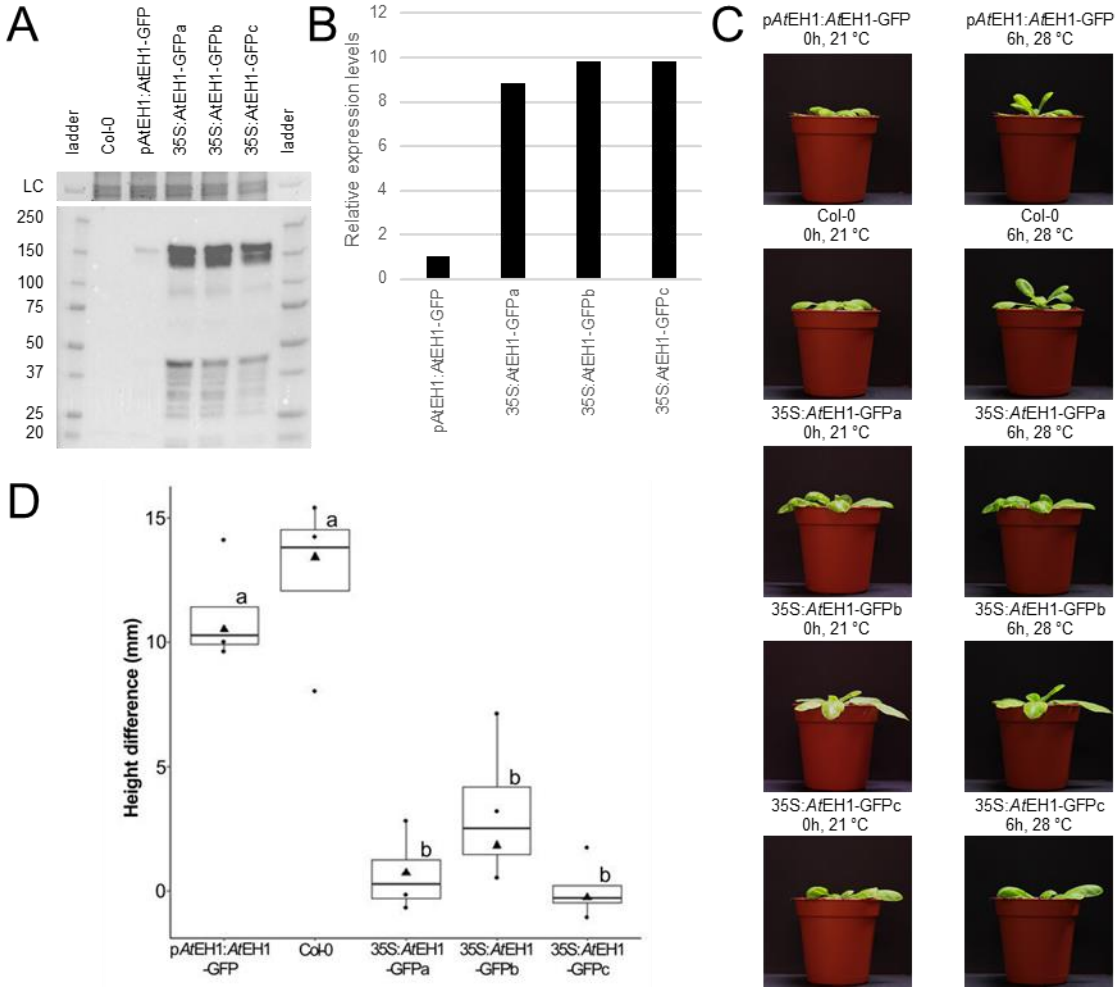

Figure 3 Western blot with anti-GFP antibody visualising the expression levels of the GFP-fused AtEH1 proteins, LC = in stain loading control (A), and quantification of the expression levels for each individual line, normalised to the AtEH1 complementation control line (pAtEH1:AtEH1-GFP) (B). Leaf hyponasty assay of 3 independent 35S:AtEH1-GFP control lines. Representative images of all lines included in this test (C). Quantification of the leaf hyponasty test. four plants were tested for each line. The triangle indicated on the box plots corresponds to the images in C. Groups with different letters are significantly different from each other ($p < 0.05$), according to a post-hoc Tukey test. The whiskers show the minimum and maximum values while the box represents the first quantile (25 %), the median and the third quantile (75 %) (D).

Differential phosphorylation of *At*EH1/Pan1 is not important for the functionality in *Arabidopsis thaliana* for root growth at 28 °C.

To test whether the functionality of *At*EH1 is altered when the protein is phospho-dead or phospho-mimicking in ten residues of the C-terminal part of the protein, I used

heterozygous *eh1-1(+/-)* mutant lines complemented with these constructs. The production of viable pollen and thus *eh1-1*(-/-) lines carrying the constructs will proof that the construct is functional under normal conditions. If this is the case, I subsequently will test whether there are differences in the phenotype at different temperatures in a root growth assay.

T2 generation plants were selected for subsequent experiments based on *At*EH1 transcript levels.

To test for complementation of the *eh1-1*(-/-) mutant, I first selected *eh1-1*(+/-) heterozygous plants in the T2 generation carrying the construct. Further selection was based on the transcript levels of the *At*EH1 gene. My aim was to select a few lines with different transcript levels. For both the phospho-dead and the phospho-mimicking mutants, I selected three lines (Figure 4). These lines were grown for self-pollination to produce T3 generation seeds

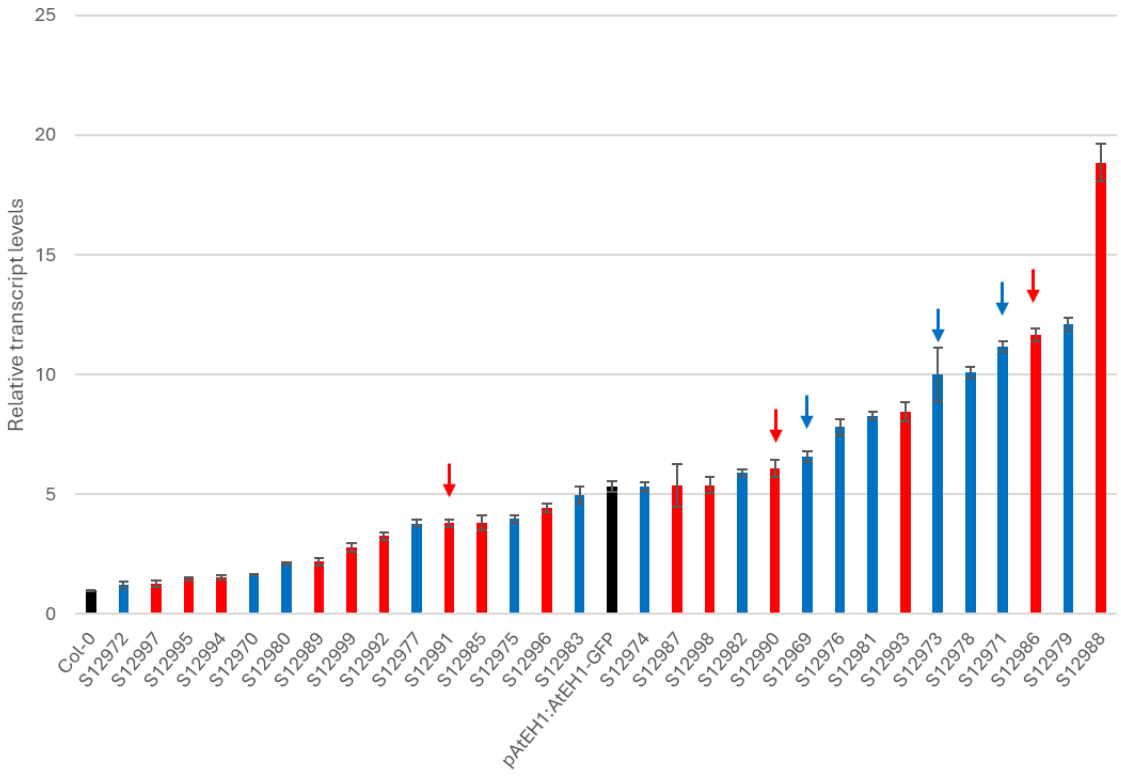

Figure 4 Transcript levels of the AtEH1 gene in the different complementation lines of the T2 generation. The transcript levels are normalised to the levels of Col-0 using CDKA as a reference gene. Col-0 and pAtEH1:AtEH1-GFP control lines are black, 10SA lines are blue, 10SD lines are red. Selected lines are marked with an arrow. The error bars represent the standard error.

Genotyping in the T3 generation allowed to identify and select *eh1-1*(-/-) mutants.

To test whether complementation of the mutant was successful, I first needed to confirm the background of my *eh1-1* plants. I am interested in plants with a homozygous mutant background (*eh1-1*(-/-)) in T3. I calculated the theoretical segregation ratio for a T2 plant heterozygous for the gene and the inserted construct (EeGg). The segregation analysis showed that the progeny of these plants should be 33.3 % wild-type, 50 % heterozygous and 16.7 % mutant (Figure 5). When I compared this with my genotyping results (Table 5 and Table 6), no line segregated according to these ratios. One possible reason is the functionality of the construct. Another possible explanation is the genotyping method that was used, since genotyping was based on negative PCR results combined with positive PCR results, I could not conclude on genotypes with full certainty. Also for some lines both PCRs didn't show a band, which also pointed in the direction of a less reliable genotyping method. For the phospho-dead *At*EH1 isoforms, I selected four lines for transcript analysis (Table 5Table 3). For the phospho-mimicking *At*EH1 isoforms, I selected eight lines for transcript analysis (Table 6).

♀ \ ♂	EG	Eg	eG	eg
EG	EEGG	EEGg	EeGG	
Eg	EEGg	EEgg	EeGg	
eG	EeGG	EeGg	eeGG	
eg	EeGg	Eegg	eeGg	

Figure 5 Punnett square for self-pollination of an eh1-1(+/-) plant heterozygous for a single locus copy of the construct. Pollen with a combination of the eg alleles are not viable and therefore they are not included in this square. E is the functional AtEH1 gene, e is the mutated AtEH1 gene, G is the functional construct, g stands for no construct. Homozygous wild-type corresponds to the grey coloured squares, heterozygous corresponds to the blue coloured squares and homozygous mutant corresponds to the green coloured squares.

Table 5 List of the genotypes of the T3 generation phospho-dead complementation lines based on two separate PCRs. For each line, the result of the PCR is given as a plus sign (band seen) or a minus sign (band not seen). The genotype was derived from the combination of the signs of the two PCRs. If both were negative, this is noted as a failed PCR. The selected lines are underlined.

Unique identifier	Construct	WT PCR	TDNA PCR	Genotype	Parental line
S13599	p*At*EH1*:At*EH1-10SA-GSL-mGFP(B)	+	+	Heterozygous	S12969
S13600	p*At*EH1*:At*EH1-10SA-GSL-mGFP(B)	+	+	Heterozygous	S12969
S13601	p*At*EH1*:At*EH1-10SA-GSL-mGFP(B)	+	+	Heterozygous	S12969
S13602	p*At*EH1*:At*EH1-10SA-GSL-mGFP(B)	+	+	Heterozygous	S12969
S13603	p*At*EH1*:At*EH1-10SA-GSL-mGFP(B)	+	+	Heterozygous	S12969
S13604	p*At*EH1*:At*EH1-10SA-GSL-mGFP(B)	+	+	Heterozygous	S12969
S13605	p*At*EH1*:At*EH1-10SA-GSL-mGFP(B)	-	-	PCR failed	S12969
S13606	p*At*EH1*:At*EH1-10SA-GSL-mGFP(B)	+	+	Heterozygous	S12969
S13607	p*At*EH1*:At*EH1-10SA-GSL-mGFP(B)	+	+	Heterozygous	S12969
S13608	p*At*EH1*:At*EH1-10SA-GSL-mGFP(B)	+	+	Heterozygous	S12969
S13609	p*At*EH1*:At*EH1-10SA-GSL-mGFP(B)	+	+	Heterozygous	S12969
S13610	p*At*EH1*:At*EH1-10SA-GSL-mGFP(B)	+	+	Heterozygous	S12969
S13611	p*At*EH1*:At*EH1-10SA-GSL-mGFP(B)	+	+	Heterozygous	S12969
S13612	p*At*EH1*:At*EH1-10SA-GSL-mGFP(B)	+	+	Heterozygous	S12969

Unique identifier	Construct	WT PCR	TDNA PCR	Genotype	Parental line
S13613	p*At*EH1:*At*EH1-10SA-GSL-mGFP(B)	-	+	Homozygous mutant	S12969
S13614	p*At*EH1:*At*EH1-10SA-GSL-mGFP(B)	-	+	Homozygous mutant	S12969
S13615	p*At*EH1:*At*EH1-10SA-GSL-mGFP(B)	-	+	Homozygous mutant	S12969
S13616	p*At*EH1:*At*EH1-10SA-GSL-mGFP(B)	+	+	Heterozygous	S12969
S13617	p*At*EH1:*At*EH1-10SA-GSL-mGFP(B)	+	+	Heterozygous	S12969
S13618	p*At*EH1:*At*EH1-10SA-GSL-mGFP(B)	-	-	PCR failed	S12971
S13619	p*At*EH1:*At*EH1-10SA-GSL-mGFP(B)	+	+	Heterozygous	S12971
S13620	p*At*EH1:*At*EH1-10SA-GSL-mGFP(B)	+	+	Heterozygous	S12971
S13621	p*At*EH1:*At*EH1-10SA-GSL-mGFP(B)	+	+	Heterozygous	S12971
S13622	p*At*EH1:*At*EH1-10SA-GSL-mGFP(B)	+	+	Heterozygous	S12971
S13623	p*At*EH1:*At*EH1-10SA-GSL-mGFP(B)	+	+	Heterozygous	S12971
S13624	p*At*EH1:*At*EH1-10SA-GSL-mGFP(B)	+	+	Heterozygous	S12971
S13625	p*At*EH1:*At*EH1-10SA-GSL-mGFP(B)	+	+	Heterozygous	S12971
S13626	p*At*EH1:*At*EH1-10SA-GSL-mGFP(B)	+	+	Heterozygous	S12971
S13627	p*At*EH1:*At*EH1-10SA-GSL-mGFP(B)	+	+	Heterozygous	S12971
S13628	p*At*EH1:*At*EH1-10SA-GSL-mGFP(B)	+	+	Heterozygous	S12971

Unique identifier	Construct	WT PCR	TDNA PCR	Genotype	Parental line
S13629	p*At*EH1:*At*EH1-10SA-GSL-mGFP(B)	+	+	Heterozygous	S12971
S13630	p*At*EH1:*At*EH1-10SA-GSL-mGFP(B)	+	+	Heterozygous	S12971
S13631	p*At*EH1:*At*EH1-10SA-GSL-mGFP(B)	+	+	Heterozygous	S12971
S13632	p*At*EH1:*At*EH1-10SA-GSL-mGFP(B)	-	+	Homozygous mutant	S12971
S13633	p*At*EH1:*At*EH1-10SA-GSL-mGFP(B)	-	-	PCR failed	S12971
S13649	p*At*EH1:*At*EH1-10SA-GSL-mGFP(B)	+	+	Heterozygous	S12989
S13650	p*At*EH1:*At*EH1-10SA-GSL-mGFP(B)	+	+	Heterozygous	S12989
S13651	p*At*EH1:*At*EH1-10SA-GSL-mGFP(B)	+	+	Heterozygous	S12989
S13652	p*At*EH1:*At*EH1-10SA-GSL-mGFP(B)	+	+	Heterozygous	S12989
S13653	p*At*EH1:*At*EH1-10SA-GSL-mGFP(B)	+	+	Heterozygous	S12989
S13654	p*At*EH1:*At*EH1-10SA-GSL-mGFP(B)	+	+	Heterozygous	S12989
S13655	p*At*EH1:*At*EH1-10SA-GSL-mGFP(B)	+	+	Heterozygous	S12989
S13656	p*At*EH1:*At*EH1-10SA-GSL-mGFP(B)	+	+	Heterozygous	S12989
S13657	p*At*EH1:*At*EH1-10SA-GSL-mGFP(B)	+	+	Heterozygous	S12989

Table 6 List of the genotypes of the T3 generation phospho-mimicking complementation lines based on two separate PCRs. For each line, the result of the PCR is given as a plus sign (band seen) or a minus sign (band not seen). The genotype was derived from the combination of the signs of the two PCRs. If both were negative, this is noted as a failed PCR. The selected lines are underlined.

Unique identifier	Construct	WT PCR	TDNA PCR	Genotype	Parental line
S13634	p*At*EH1:*At*EH1-10SD-GSL-mGFP(B)	+	+	Heterozygous	S12986
S13635	p*At*EH1:*At*EH1-10SD-GSL-mGFP(B)	+	+	Heterozygous	S12986
S13636	p*At*EH1:*At*EH1-10SD-GSL-mGFP(B)	+	+	Heterozygous	S12986
S13637	p*At*EH1:*At*EH1-10SD-GSL-mGFP(B)	-	-	PCR failed	S12986
S13638	p*At*EH1:*At*EH1-10SD-GSL-mGFP(B)	+	+	Heterozygous	S12986
S13639	p*At*EH1:*At*EH1-10SD-GSL-mGFP(B)	+	+	Heterozygous	S12986
S13640	p*At*EH1:*At*EH1-10SD-GSL-mGFP(B)	+	+	Heterozygous	S12986
S13641	p*At*EH1:*At*EH1-10SD-GSL-mGFP(B)	-	+	Homozygous mutant	S12986
S13642	p*At*EH1:*At*EH1-10SD-GSL-mGFP(B)	+	-	Homozygous wild-type	S12986
S13643	p*At*EH1:*At*EH1-10SD-GSL-mGFP(B)	-	+	Homozygous mutant	S12986
S13644	p*At*EH1:*At*EH1-10SD-GSL-mGFP(B)	+	+	Heterozygous	S12986
S13645	p*At*EH1:*At*EH1-10SD-GSL-mGFP(B)	-	-	PCR failed	S12986
S13646	p*At*EH1:*At*EH1-10SD-GSL-mGFP(B)	+	+	Heterozygous	S12986
S13647	p*At*EH1:*At*EH1-10SD-GSL-mGFP(B)	-	+	Homozygous mutant	S12986

Unique identifier	Construct	WT PCR	TDNA PCR	Genotype	Parental line
S13648	p*At*EH1:*At*EH1-10SD-GSL-mGFP(B)	+	+	Heterozygous	S12986
S14160	p*At*EH1:*At*EH1-10SD-GSL-mGFP(B)	+	+	Heterozygous	S12990
S14161	p*At*EH1:*At*EH1-10SD-GSL-mGFP(B)	+	+	Heterozygous	S12990
S14162	p*At*EH1:*At*EH1-10SD-GSL-mGFP(B)	+	+	Heterozygous	S12990
S14163	p*At*EH1:*At*EH1-10SD-GSL-mGFP(B)	+	+	Heterozygous	S12990
S14164	p*At*EH1:*At*EH1-10SD-GSL-mGFP(B)	-	+	Homozygous mutant	S12990
S14165	p*At*EH1:*At*EH1-10SD-GSL-mGFP(B)	+	+	Heterozygous	S12990
S14166	p*At*EH1:*At*EH1-10SD-GSL-mGFP(B)	+	+	Heterozygous	S12990
S14167	p*At*EH1:*At*EH1-10SD-GSL-mGFP(B)	+	+	Heterozygous	S12990
S14168	p*At*EH1:*At*EH1-10SD-GSL-mGFP(B)	-	+	Homozygous mutant	S12990
S14169	p*At*EH1:*At*EH1-10SD-GSL-mGFP(B)	+	+	Heterozygous	S12990
S14170	p*At*EH1:*At*EH1-10SD-GSL-mGFP(B)	-	+	Homozygous mutant	S12990
S14171	p*At*EH1:*At*EH1-10SD-GSL-mGFP(B)	+	+	Heterozygous	S12990
S14172	p*At*EH1:*At*EH1-10SD-GSL-mGFP(B)	+	+	Heterozygous	S12990
S14173	p*At*EH1:*At*EH1-10SD-GSL-mGFP(B)	+	+	Heterozygous	S12990
S14175	p*At*EH1:*At*EH1-10SD-GSL-mGFP(B)	+	-	Homozygous wild-type	S12990

Unique identifier	Construct	WT PCR	TDNA PCR	Genotype	Parental line
S14176	p*At*EH1:*At*EH1-10SD-GSL-mGFP(B)	+	+	Heterozygous	S12990
S14177	p*At*EH1:*At*EH1-10SD-GSL-mGFP(B)	+	+	Heterozygous	S12990
S14178	p*At*EH1:*At*EH1-10SD-GSL-mGFP(B)	+	-	Homozygous wild-type	S12991
S14179	p*At*EH1:*At*EH1-10SD-GSL-mGFP(B)	+	+	Heterozygous	S12991
S14180	p*At*EH1:*At*EH1-10SD-GSL-mGFP(B)	+	+	Heterozygous	S12991
S14181	p*At*EH1:*At*EH1-10SD-GSL-mGFP(B)	+	+	Heterozygous	S12991
S14182	p*At*EH1:*At*EH1-10SD-GSL-mGFP(B)	+	+	Heterozygous	S12991
S14183	p*At*EH1:*At*EH1-10SD-GSL-mGFP(B)	-	+	Homozygous mutant	S12991
S14184	p*At*EH1:*At*EH1-10SD-GSL-mGFP(B)	-	+	Homozygous mutant	S12991
S14185	p*At*EH1:*At*EH1-10SD-GSL-mGFP(B)	-	+	Homozygous mutant	S12991
S14186	p*At*EH1:*At*EH1-10SD-GSL-mGFP(B)	-	+	Homozygous mutant	S12991

T3 generation plants for subsequent experiments were selected based on the *At*EH1 transcript level.

I selected the *eh1-1*(-/-) lines in the previous test, now my goal is to select lines with a transcript level similar to the transcript level of the control line p*At*EH1:*At*EH1-GFP, which is the endogenous gene under the control of the endogenous promoter. For each of the phospho-mutants, I selected two independent lines to test if the phenotype is complemented at different temperatures (Figure 6).

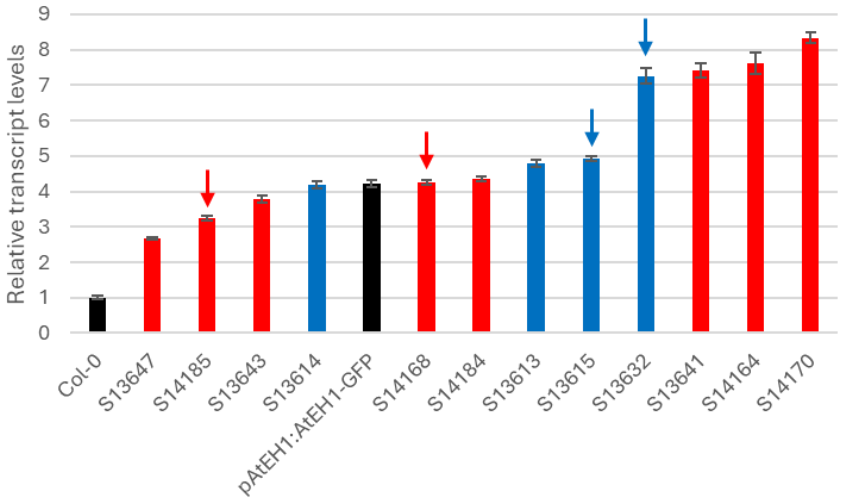

Figure 6 Transcript levels of the AtEH1 gene in the different complementation lines of the T3 generation. The transcript levels were normalised with Col-0 using CDKA as a reference gene. Col-0 and pAtEH1:AtEH1-GFP control lines are black, 10SA lines are blue, 10SD lines are red. Selected lines are marked with an arrow. The error bars represent the standard error.

A root growth assay showed no unaltered functionality of phospho-mutated *At*EH1 proteins at temperatures of 28 °C.

Since CME is important for plant growth and development, I tested the complementation lines in a root growth assay to see if the construct is defective at 28 °C. For this test, I included wild-type Col-0 and the complementation line containing the full length AtEH1 under the control of the endogenous promoter (pAtEH1:AtEH1-GFP) as control. The seeds were all grown at 21 °C before transferring to two different temperatures. I did this to prevent the analysis of seeds germinating later during the experiment. Non- and late-germinated seeds were excluded from the analysis. Images were taken after the incubation period for the quantification (Figure 7B). The root growth assay was quantified by measuring the difference in root growth from the mark until the new position of the root

tip (Figure 7A). A post-hoc multiple comparisons test showed that the root growth of phospho-dead lines does not significantly differ from the root growth of Col-0 at 21 °C. While this test showed that the root growth of phospho-mimicking lines did significantly differ from the root growth of Col-0 at 21 °C. At 28 °C the results were not unanimous for

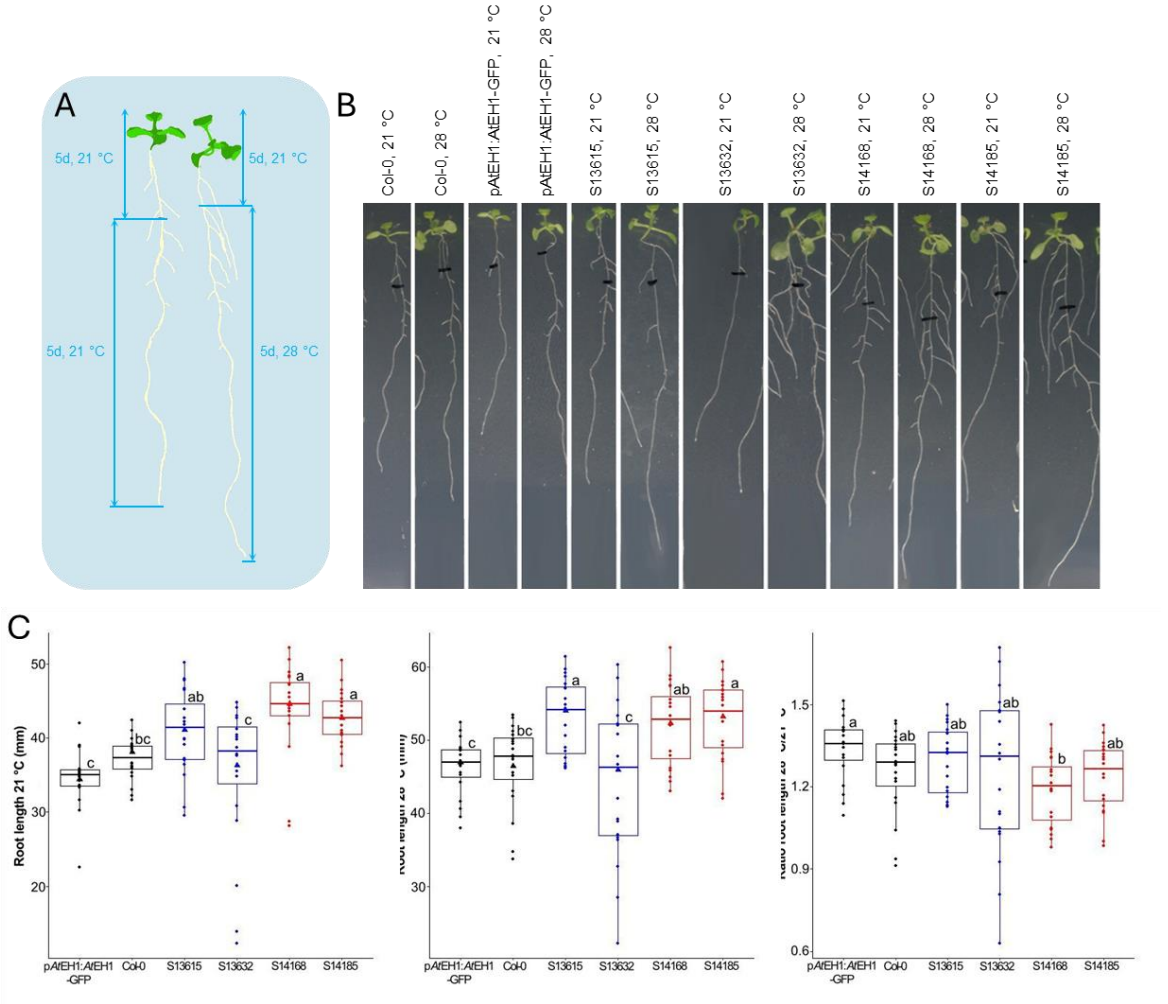

Figure 7 Root growth assay of phospho-dead and phospho-mimicking AtEH1 proteins expressed in eh1-1(-/-) mutant lines. Diagram of two seedlings, each grown at 21 °C for five days and then transferred. Before transferring the position of the root tip after five days is marked. The seedlings are moved to 21 °C and to 28 °C for five days. After this period, the length of the root is measured from the mark-up until the root tip (A). Representative images of seedlings of each line. For each line two seedlings are shown, one grown at each temperature (B). The quantification of the root growth is shown in these boxplots for each line at each temperature. The ratio between both measurements is calculated for each measurement at 28 °C divided by the average of the root growth of that line at 21 °C. Data points shown as a triangle on the plots represent the pictures shown in B. Groups with different letters are significantly different from each other ($p<0.05$) according to a post-hoc multiple comparisons test. The whiskers show the minimum and maximum values while the box represents the first quantile (25 %), the median and the third quantile (75 %) (C).

both independent lines of each phospho-mutant. For both mutants, one independent line showed significant differences with the Col-0 wild type while the other did not. To conclude on the functionality of the mutated protein at temperatures of 28 °C, I normalised each measurement with the average measurement of each line at 21 °C to produce a ratio (Figure 7C). This showed that there were no significant differences between the Col-0 wild type and the tested mutant lines. I conclude that the functionality of the *At*EH1 protein is not affected by the ten phospho-mutations in a root growth assay at 21 °C and at 28 °C.

DISCUSSION

In this study, I tested the hypothesis stating there is a relationship between temperature-mediated phosphorylation of *At*EH1/Pan1 and hyponasty. I also tested whether the phospho-mutations affected the functionality of *At*EH1/Pan1 at 28 °C. Overexpression lines and complementation lines were used to test the hypothesis and the additional research question, respectively. I found no significant differences between the Col-0 control line and the phospho-dead and phospho-mimicking overexpression lines in the hyponasty assay. I conclude one or more of the ten residues investigated in my study might be linked to temperature-mediated leaf hyponasty. I found no significant differences between the Col-0 control line and the tested complementation lines in a root growth assay at 21 °C and at 28 °C. I conclude there is no functional impairment of the *At*EH1 protein due to the phospho-mutations observed in my experimental set-up.

Temperature-mediated phosphorylation plays a role in regulating hyponasty.

The hyponasty test revealed no significant differences between the wild-type control line and the phospho-dead and phospho-mimicking overexpression lines. However, I observed a significant difference between the 35S:*At*EH1-GFP overexpression control line and the phospho-dead and phospho-mimicking overexpression lines (Figure 2). The abolishment of the unresponsive phenotype of the overexpression mutant lines, indicates there might be a relationship between temperature-dependent phosphorylation and hyponasty.

The 35S:*At*EH1-GFP line, used as a control, doesn't show hyponasty at 28 °C after a growth period of 6 hours at this temperature. The phenotype in the 35S:*At*EH1-GFP line could be caused by the overexpression of the protein. In my experiments, I tested different phospho-mutant lines with higher, similar or lower expression levels compared to the 35S:*At*EH1-GFP line. These lines didn't show the same phenotype. I see two differences between the control line and the phospho-mutant lines that could be responsible for the difference in phenotype. First, the insertion site of the construct is different for all lines. To exclude this as the reason for the different phenotypes, the 35S:*At*EH1-GFP control line was tested together with two other independent lines overexpressing the native *At*EH1 gene. The three lines had similar expression levels and all showed the defective hyponasty phenotype (Figure 3). I conclude that the site of insertion is not the causal agent for the phenotypic difference between the overexpression control line and the overexpression phospho-mutant lines.

Secondly, the native *At*EH1 protein has a phosphorylation switch, phosphorylation and dephosphorylation can occur, whereas the phospho-mutants are phospho-dead or phospho-mimicking in ten residues of the C-terminus. I saw that an *At*EH1 overexpression line did not respond to an increase in temperature, whereas the phospho-mutant overexpression lines responded to an increase in temperature in the same way as a Col-0 wild type control line. The *At*EH1 phospho-dead and phospho-mimicking lines abolish the unresponsive phenotype of the *At*EH1 overexpression line. This suggests that blocking the phosphorylation switch at one or more of the ten residues tested is responsible for abolishing the non-responsiveness phenotype. A similar observation for both phospho-dead and phospho-mimicking mutants leads us to hypothesise that amino acid substitutions to create a phospho-mimicking residue may not have the same effect on the protein and the molecular mechanisms in the cell as an actual phosphorylation of the protein. Previously, phospho-mimicking residues not acting quite like actual phosphorylation has been observed before in a phospho-mimicking validation study. Phosphorylated and phospho-mimicking 14-3-3 proteins were compared in human cancer cell lines. Phosphorylated proteins were produced using a mouse kinase that specifically recognises a motif around position 58 of the protein. The phospho-mimicking proteins used were S58E, S58D and S57D_S58D. The last phospho-mimicking mutant

was included because a phosphate group has a higher negative charge than the phospho-mimicking Asp and Glu amino acids. The addition of an extra phospho-mimicking residue may be more realistic in mimicking phosphorylation. This research concluded that there is a shift in the dimer-monomer equilibrium of phosphorylated and phospho-mimicking mutants. Other physical properties such as melting temperature and hydrophobicity were significantly different between phosphorylation and phospho-mimicry. The use of the S57D_S58D mutant has shown that its behaviour is more comparable to phosphorylation (Kozeleková et al., 2022). Although this study suggests the use of a double negative charge to more accurately mimic phosphorylation. They only had one phosphorylation site to account for, my study would need to account for ten phosphorylation sites, and changing multiple amino acid residues at these ten positions could have a detrimental effect on the protein properties.

A better solution to further investigate the idea that the causative phosphorylation site is one of these ten tested sites would be to focus on the phospho-dead mutants. I could create new lines with fewer mutated phospho-dead sites. In this way, I can gradually re-activate the phosphorylation switch site by site and test the plant phenotype for each of the new mutants. Using this method, and making sure that I use lines with expression levels that are equal to the 35S:*At*EH1-GFP lines, I might be able to see which site is causing the unresponsive phenotype due to the re-activation of the phosphorylation switch. Another possibility is to generate 10 mutant lines, each with one phospho-dead residue. These approaches can identify one causative amino acid residue, but if several residues interact with each other, the phosphosites of interest would have to be combined.

When testing this further in the future, I need to bear in mind that the phosphorylation of different residues could have a positive or negative effect on each other. The co-operation of different phosphorylated residues was also observed in a study of nitrate uptake by NRT2.1. They discovered at least five phosphorylation sites in the nitrate transporter NRT2.1 that influence nitrate uptake. Depending on the phosphorylation state of the site, nitrate uptake is regulated or not. For two of these sites, they found that single phosphorylation had a positive effect on nitrate influx activity, whereas double

phosphorylation, had a negative effect on nitrate influx. A double dephosphorylated mutant was also included in the study. This protein was unstable and had a high turnover rate (Li et al., 2024). This type of effect needs to be taken into account when further investigating the effect of *At*EH1 phosphorylation on leaf hyponasty.

Although I had previously concluded that mutant lines with different expression levels showed a different phenotype than the 35S:*At*EH1-GFP line, it would be interesting to test lines with higher expression levels to see if I could manipulate the phenotype. In my expression analysis, I found that excessive expression levels were not present in the lines currently obtained. Lines in which the construct is inserted into multiple loci could be used for this purpose. The disadvantage of this method is that there is no control over the number of insertions or the stability of the expression levels. Another way to obtain high expressing lines is to cross two of the homozygous T3 lines with high expression levels. The progeny of this cross should carry the construct at two different loci. This approach is more controlled. This experiment could also be done the other way round if I would make 35S:*At*EH1-GFP lines with lower expression levels and then see if these lines lift their leaves at 28 °C or not.

Disabling the phosphorylation switch in *At*EH1 doesn't impact its functionality in a root growth experiment at 21 °C and 28 °C.

To answer the research question of whether the *At*EH1 phospho-mutants are functionally affected at high ambient temperatures, I used complemented *eh1-1* mutant lines. I observed no significant differences in root growth between the Col-0 control line and the phospho-mutant complemented lines (Figure 7). I conclude that there is no loss of function of the phospho-mutated *At*EH1 protein observed in a root growth assay at 28 °C compared to 21 °C. I have only tested the complementation lines in one assay and further tests should be carried out to draw further conclusions on the functionality of the phospho-mutated *At*EH1 protein at high ambient temperatures. As CME is involved in plant growth and development, it is also interesting to further test development-related phenotypes as well such as flowering time, fecundity and plant architecture. Scheepens et al. (2018) investigated eleven genotypes of *Arabidopsis thaliana* for several phenotypes under temperature stress at 30 °C compared to 20 °C. Depending on the

genotype, the researchers saw negative, weak negative, positive and no response to the continuous temperature stress. Next to continuous stress, they tested six temperature fluctuation treatments. Each with another timing and frequency of stress. This part of the experiment showed that the timing during development affected performance more than the frequency of temperature stress (Scheepens et al., 2018). The complementation lines can be further tested for different development phenotypes such as flowering time, fecundity and plant architecture, both with a continuous temperature stress influx and with a well-timed temperature stress influx.

Although the experimental set-up of the root growth assay was designed to optimise the analysis of root growth differences between 21 °C and 28 °C by eliminating the inclusion of seeds that germinated later during incubation, there were still some limitations that became apparent during the data-analysis. The data were not normally distributed, which could be avoided in the future by testing more than twenty seedlings. In my boxplots, I observed that the variance of some of the lines was large, which is also not ideal for drawing conclusions. This could be solved by testing more seedlings in the future. Another possibility would be to check other lines that met the selection criteria to see if the variation of these lines is less.

Another limitation in my experiments selecting the lines for the root growth experiment is the genotyping method used. Two PCRs were used to determine the genotype of the *eh1-1* mutants. This means that a homozygous genotype is characterised by a positive and a negative PCR result. The problem here lays within the negative PCR result, since there are several other options for a PCR to be negative than solely the fact that the gene is not present. It is possible that a result is a false negative, the product of interest is present in the sample, but cannot be detected. There are multiple causes for this problem such as a non-accurate Mg^{2+}-concentration, a wrong annealing temperature, unintentionally not adding a component, wrong amount of DNA added… (Lorenz, 2012). A PCR could also fail due to components inhibiting the reaction. The genotyping results were not consistent with the predicted ratios based on a segregation analysis. This indicates that either the genotyping method failed or that there is something wrong with the plant lines. In the future, I could narrow down the cause of the issue by using other

methods than the PCR-based genotyping to draw conclusions on the background of the *eh1-1* mutants. For example, the plants can be grown to produce pollen, a viability stain such as FDA can then be used on the pollen to determine the pollen viability. If the construct is not functional or there is no construct inserted in the *eh1-1*(+/-) mutants, a ratio of 1:1 viable:non-viable pollen should be observed. Insertion of a functional construct in the *eh1-1*(+/-) mutants has a ratio deviating from the 1:1 ratio (Gadeyne et al., 2014). A protein analysis of the native *At*EH1 protein through Western blot with the use of an anti-EH1 antibody is another possibility to analyse the *eh1-1* mutants. This test targets the native *At*EH1 gene. As the antibody targets the C-terminal end of the native protein, the A*t*EH1 isoform, with ten phospho-dead or phospho-mimicking residues in its C-terminal end, cannot be visualised with the antibody. If this is combined with a western blot using anti-GFP antibody, I would be able to draw conclusions on homozygosity and heterozygosity of the *eh1-1* mutants like I did with the results of the PCR genotyping.

In conclusion, I have shed some light on the relationship between temperature-dependent phosphorylation of *At*EH1 and temperature-mediated leaf hyponasty. However, there are still interesting questions to be investigated in the future. Which kinase regulates the phosphorylation switch in *At*EH1/Pan1 and is it only one kinase or are several kinases involved? What is the relationship between phosphorylated *At*EH1/Pan1 and clathrin-mediated endocytosis? *At*EH1/Pan1 is also differentially phosphorylated at cold temperatures, what is the function of this phosphorylation and is it related to CME? Will we be able to study protein phosphorylation more accurately than with phospho-mimicry? Further research is needed to answer all these questions.

METHODS

Plant material

Arabidopsis thaliana ecotype Col-0 was used for all experiments. Overexpression lines used in this study consist of Col-0 plants carrying phospho-dead and phospho-mimicking EH1 genes under the strong constitutive 35S promoter. Overexpression lines at the second (T2) and third (T3) generations were used. The control plants for these lines were wild-type Col-0 plants and Col-0 plants carrying the endogenous EH1 gene under the strong constitutive promoter 35S.

To generate the complementation lines, phospho deficient and phospho mimetic variants of *At*EH1/Pan1-GFP (by substituting the identified serine sites with alanine or aspartic acid, respectively) were synthesised using site-directed mutagenesis via direct DNA synthesis (Twist Bioscience). Then, the 2356 bp EH1 promoter and 5'UTR were fused to the CDS of phospho-dead and phospho-mimicking EH1 and mGFP using Golden Gate cloning. Transformed via floral dip (Clough and Bent, 1998) into plants heterozygous for the *eh1-1*(+/-) T-DNA (SALK 083997) (Gadeyne et al., 2014). Positive transformants were screened on ½ MS plates supplemented with Basta (20 mg/l). Heterozygous *eh1-1*(+/-) plants were selected by genotyping, and in the following generation seedlings homozygous for *eh1-1(-/-)* were identified. Complementation lines at the second (T2) and third (T3) generations were used. The control plants for these lines were wild-type Col-0 plants and *eh1-1*(-/-) plants carrying the endogenous EH1 gene under the endogenous promoter EH1.

Plant growth and selection

Seeds were surface sterilised with chlorine gas and grown on ½ Murashige and Skoog (½ MS) plates (4.2 g/l MS (Murashige and Skoog, 1962), 1 g/l MES, 0.2 g/l myo-inositol, 0.4 % agar, no sucrose, pH 5.7). Seeds were sown in a sterile environment on ½ MS plates supplemented with Basta (20 mg/l) for selection. The plates were stratified at 4 °C for 2 days. After stratification, the plates were placed in a vertical position in the growth room (continuous light, 75 µE m^{-2} s^{-1}, 21 °C) for germination and further growth.

RNA extraction and RT-qPCR analysis

Twenty whole 7-day-old seedlings were harvested for RNA extraction. The material was ground with a Retsch MM 400 at a frequency of 20/s for 1 minute. RNA was extracted with the ReliaPrep™ RNA Tissue Miniprep System (Promega) according to the protocol for non-fibrous tissue (Promega, 2016) included. The RNA was measured with a NanoDrop™ One (Thermo Fisher Scientific).

1 µg of the RNA template was mixed with 5x qScript Master Mix (QuantaBio) and diluted with nuclease-free water in an end volume of 20 µl. A thermocycler (Bio-Rad) was used with the following protocol: 5 minutes priming at 25 °C, 30 minutes reverse transcription at 42 °C, 5 minutes RT inactivation at 85 °C, hold at 4 °C.

The Janus pipetting robot was used to make the reagent mix for the qPCR. The cDNA was diluted five times to load the pipetting robot. The qPCR primers (Table 7) were mixed in a final concentration of 1.5 µM to load the pipetting robot. Sybr Green I master mix (Roche) was loaded in the Janus pipetting robot. qPCR was run with a LightCycler® 480 (Roche).

Table 7 List of primers

Purpose	Primer name	Sequence
qPCR	Actin 7 forward primer	5'-GGAAACATCGTTCTCAGTGGT-3'
qPCR	Actin 7 reverse primer	5'-CTTGATCTTCATGCTGCTAGGT-3'
qPCR	CDKA forward primer	5'-ATTGCGTATTGCCACTCTCATAGG-3'
qPCR	CDKA reverse primer	5'-TCCTGACAGGGATACCGAATGC-3'
qPCR	*At*EH1/Pan1 forward primer	5'- GTCGCTTTCTGATCGGTCAC-3'
qPCR	*At*EH1/Pan1 reverse primer	5'- TAGCAGCAGGATTAGGTCGG-3'
Genotyping	*At*EH1/Pan1 LP	5'-TGCAGCAGAAATTGTTCTGG-3'
Genotyping	*At*EH1/Pan1 RP	5'-ATGAGACCACCAGTTCCTGC-3'
Genotyping	T-DNA LP	5'-ATTTTGCCGATTTCGGAAC-3'

DNA extraction and genotyping

Twenty whole 7-day-old seedlings were harvested for DNA extraction. The material was ground with a Retsch MM 400 at a frequency of 20/s for 1 minute. DNA was extracted with the Wizard® Genomic DNA purification kit. The protocol from the kit (Promega, 2023) was followed according to a modification. The volumes of the different reagents, except for the DNA rehydration solution, were halved. Additionally, the first centrifugation step was prolonged to 10 minutes instead of 3 minutes for a better separation of supernatant and cell debris.

For genotyping, the extracted DNA was amplified through two separate PCR reactions. The first PCR was used to check the presence of the WT EH1 with gene-specific primers (Table 7), bands with a length of 958 bp were expected. The second PCR was used to

check the presence of T-DNA in the EH1 gene, with one gene-specific primer and a primer specific for the T-DNA insertion (Table 7), bands with a length of 550 bp were expected. 1 µl of DNA was mixed with master mix (1x GoTaq® Reaction Buffer, 3 mM $MgCl_2$, 0.4 µM forward primer, 0.4 µM reverse primer, 0.2 mM dNTPs, 1.25 U GoTaq® enzyme) in a final volume of 15 µl. A thermocycler (Bio-Rad) was used for touchdown genotyping (Table 8 and Table 9). The PCR products together with a DNA ladder (1 kb, Benchtop) were loaded in a 1% agarose gel (UltraPure™ Agarose, Invitrogen) supplemented with SYBR™ Safe DNA Gel Stain (0.006%, Invitrogen). The gel was run at 100 V for 12 minutes and imaged using the Gel Logic 100 Imaging System (Kodak).

Table 8 Thermocycler program for amplification of the WT AtEH1 gene

Temperature	Time	Amount of cycles
95 °C	2:00	1x
95 °C	0:30	
65 °C (- 1 °C per cycle)	0:20	13x
72 °C	2:00	
95 °C	0:30	
52 °C	0:20	25x
72 °C	2:00	
72 °C	5:00	1x
4 °C	Hold	

Table 9 Thermocycler program for amplification of the T-DNA inserted AtEH1 gene

Temperature	Time	Amount of cycles
95 °C	2:00	1x
95 °C	0:30	
65 °C (- 1 °C per cycle)	0:20	10x
72 °C	1:00	
95 °C	0:30	
55 °C	0:20	25x
72 °C	1:00	
72 °C	5:00	1x
4 °C	Hold	

Western blot

7-day-old seedlings were harvested and flash frozen in liquid nitrogen. The plant material was ground with liquid nitrogen until a fine powder was obtained to extract the proteins. 100 µg of ground leaf material was mixed with extraction buffer (50 mM Tris/HCl pH 7.6, 15 mM $MgCl_2$, 150 mM NaCl, 60 mM β-glycerophosphate, 0.1 mM Na_3VO_4, 1 mM NaF, 1 mM PMSF, 1 tablet/50 ml Complete™ ultra EDTA-free (Roche), 1 µM E64, 0.5 mM EDTA, 0.10 % NP40, 5% ethylene glycol) in a ratio 1:2 and incubated for 60 minutes at 4 °C. The samples were centrifuged twice at 14000 rpm for 10 minutes at 4 °C. The supernatant was transferred to fresh tubes. To measure the protein concentration, Qubit™ protein buffer (Invitrogen) and Qubit™ protein reagents (Invitrogen) (199:1) were mixed, and 1 µl of each sample was mixed and added in the mixed buffer (199 µl) to an end volume of 200 µl . This mixture was incubated for 15 minutes at room temperature and measured with a Qubit™ 2.0 fluorometer (Invitrogen). The samples were equalised based on the measured protein concentration by dilution with the extraction buffer in a total volume of 50 µl. 20 µl of Laemmli sample buffer (4x, Bio-Rad) and 8 µl of NuPAGE™ Sample reducing agent (10x, Invitrogen) were mixed in a volume of 28 µl to add to the samples of 50 µl. The samples were heated at 90 °C for 10 minutes.

The mini-PROTEAN TGX Stain-free gel (4-20%, 15 wells, 15 µl/well) (Bio-Rad) was mounted in a gel electrophoresis chamber for western blot. The gel was submerged in Tris/Glycine/SDS buffer (Bio-Rad). 5 µl of ladder (Precision Plus Protein™ All Blue Standards (Bio-Rad) and Precision Plus Protein™ Unstained Standards (Bio-Rad), 1:1) and 12 µl of samples were loaded in the gel. The gel was run at 180 V for 40 minutes with a PowerPac™ HC High-Current Power Supply (Bio-Rad). The stain-free gel was imaged using the ChemiDoc Imaging System (Bio-Rad), with the settings application Stain Free Gel, 590/110, UV Trans under Auto Optimal exposure. The gel was prepared for blotting with the Trans-Blot Turbo Transfer Pack (Bio-Rad) according to the protocol included in the kit (Bio-Rad Laboratories, 2018). The Trans-Blot Turbo Transfer System (Bio-Rad) was used at 12 V for 7 minutes for blotting.

After blotting, the blot was blocked using skim milk (2.5 g in 50 ml PBS-T (0.1% Tween-20)) for at least one hour at 4 °C. The blot was incubated with anti-GFP antibody (1:1000 in skim milk, GFP Antibody HRP, Miltenyi Biotech) for at least one hour. The blot was washed three times in PBS-T for 10 minutes. After washing, the blot was drained in Enhanced Luminol Reagent Plus (PerkinElmer) and Oxidizing Reagent Plus (PerkinElmer) in a ratio of 1:1 for visualisation. The blot was stored in the dark and visualised with the ChemiDoc Imaging System (Bio-Rad), with the settings application colorimetric to visualise the ladder and the settings chemiluminescence to visualise the antibody both under Auto Optimal exposure. The amount of protein was quantified with the program ImageJ ((Schindelin et al., 2012), version Java 1.8.0_172, 64-bit).

Hyponasty assay

Pots of soils (Saniflor soil for sowing and cuttings) were filled to the brim and water soaked a day before transferring 7-day-old seedlings to soil. The plants were further grown in the growth room (16h/8h light/dark, 113 µE m^{-2} s^{-1}, 21 °C) for two weeks. The plants were placed at 28 °C in a Lovibond (105 µE m^{-2} s^{-1}) at continuous light for 6 hours. The front view of the plants was captured before (timepoint 0 hours, 0h) and after (timepoint 6 hours, 6h) the incubation period to determine the movement of the leaves. The pictures were analysed with ImageJ ((Schindelin et al., 2012), version

Java 1.8.0_172, 64-bit), for all pictures the distance between the top of the pot and the top of the highest leaf was measured, the same leaf was measured at 0h and 6h.

Root growth assay

Seeds were sown equally spaced on plates with 50 ml ½ MS. After stratification, the plates were placed in the growth room (continuous light, 75 µE m^{-2} s^{-1}, 21 °C) for five days. The seedlings were placed on fresh plates in an orderly manner and the end of the root was marked on the plate. The amount of plates was divided and placed in a Lovibond at 21 °C or 28 °C. After five days an image was taken. The images were analysed with the plug-in NeuronJ in the program ImageJ ((Schindelin et al., 2012), version Java 1.8.0_172, 64-bit) to check the difference in root growth.

Statistics

The segregation ratio of the overexpression lines was tested with a Chi-Square test to see if they differ from the expected ratio of 3:1. The formula (1) is used.

$$\chi^2 = \frac{\sum(O_i - E_i)^2}{E_i} \quad (1)$$

$$\text{where } O_i = \text{ observed value (actual value)}$$

$$\text{and } E_i = \text{ expected value.}$$

The leaf movement in the hyponasty assay was evaluated using ANOVA followed by a post-hoc Tukey's HSD-test. RStudio (RStudio 2024.04.1+748 "Chocolate Cosmos" Release for windows) was used for this analysis.

The difference in root growth in the root growth assay was evaluated using a Kruskal Wallis statistical test followed by multiple pairwise-comparison as post-hoc test. RStudio (RStudio 2024.04.1+748 "Chocolate Cosmos" Release for windows) was used for this analysis.

ACKNOWLEDGEMENTS

I am grateful to Prof. Dr. ir. Daniel Van Damme for letting me join his lab. His guidance and mentorship throughout the course of my thesis have been invaluable. Thanks also to Tingyu Zhu, who helped me in the lab and with my thesis. I am thanking Michaël

Vandorpe who also helped with the set-up of some of the experiments. Further, I thank the whole lab group for making me feel welcome and being supportive. The nice atmosphere and collaborative spirit have helped me in my academic pursuits.

I am thankful to my parents for supporting me and providing me with the opportunity to obtain an additional master's degree. Their belief in me and my abilities has helped me a lot throughout the course of the past year. Finally, I want to thank my friends and my boyfriend for their encouragement and support. Their company and understanding made the journey easier.

REFERENCES

Bashline, L., Li, S., Anderson, C. T., Lei, L., & Gu, Y. (2013). The endocytosis of cellulose synthase in arabidopsis is dependent on μ2, a clathrin-mediated endocytosis adaptin. *Plant Physiology*, *163*(1), 150–160. https://doi.org/10.1104/pp.113.221234

Bio-Rad Laboratories. (2018). *Trans-Blot Turbo Transfer System Transfer Pack Quick Start Guide Instructions for Using Trans-Blot Turbo Transfer Packs*.

Clough, S. J., & Bent, A. F. (1998). Floral dip: A simplified method for Agrobacterium-mediated transformation of Arabidopsis thaliana. *Plant Journal*, *16*(6), 735–743. https://doi.org/10.1046/j.1365-313X.1998.00343.x

Dragwidge, J. M., Wang, Y., Brocard, L., De Meyer, A., Eeckhout, D., Grones, P., Buridan, M., Chambaud, C., Potocký, M., Winkler, J., Vandorpe, M., Serre, N., Fendrych, M., Bernard, A., De Jaeger, G., Pleskot, R., Fang, X., & Van Damme, D. (2024). *Biomolecular condensation orchestrates clathrin-mediated endocytosis in plants*.

Fujimoto, M., Arimura, S. I., Ueda, T., Takanashi, H., Hayashi, Y., Nakano, A., & Tsutsumi, N. (2010). Arabidopsis dynamin-related proteins DRP2B and DRP1A participate together in clathrin-coated vesicle formation during endocytosis. *Proceedings of the National Academy of Sciences of the United States of America*, *107*(13), 6094–6099. https://doi.org/10.1073/pnas.0913562107

Gadeyne, A., Sánchez-Rodríguez, C., Vanneste, S., Di Rubbo, S., Zauber, H., Vanneste, K., Van Leene, J., De Winne, N., Eeckhout, D., Persiau, G., Van De Slijke, E., Cannoot, B., Vercruysse, L., Mayers, J. R., Adamowski, M., Kania, U., Ehrlich, M., Schweighofer, A., Ketelaar, T., … Van Damme, D. (2014). The TPLATE adaptor complex drives clathrin-

mediated endocytosis in plants. *Cell*, *156*(4), 691–704. https://doi.org/10.1016/j.cell.2014.01.039

Grones, P., De Meyer, A., Pleskot, R., Mylle, E., Kraus, M., Vandorpe, M., Yperman, K., Eeckhout, D., Dragwidge, J. M., Jiang, Q., Nolf, J., Pavie, B., De Jaeger, G., De Rybel, B., & Damme, D. Van. (2022). *The endocytic TPLATE complex internalizes ubiquitinated plasma membrane cargo Europe PMC Funders Group*.

Johnson, A., Dahhan, D. A., Gnyliukh, N., Kaufmann, W. A., Zheden, V., Costanzo, T., Mahou, P., onika Hrtyan, M., Wang, J., Aguilera-Servin, J., Van Damme, el, Beaurepaire, E., Loose, M., Bednarek, S. Y., & 1 Friml, J. (2021). The TPLATE complex mediates membrane bending during plant clathrin-mediated endocytosis. *PNAS*, *118*(51). https://doi.org/10.1073/pnas.2113046118/-/DCSupplemental

Johnson, A., & Vert, G. (2017). Single event resolution of plant plasma membrane protein endocytosis by TIRF microscopy. *Frontiers in Plant Science*, *8*. https://doi.org/10.3389/fpls.2017.00612

Kim, J. Y., Park, Y. J., Lee, J. H., & Park, C. M. (2019). Developmental polarity shapes thermo-induced nastic movements in plants. *Plant Signaling and Behavior*, *14*(8). https://doi.org/10.1080/15592324.2019.1617609

Kozeleková, A., Náplavová, A., Brom, T., Gašparik, N., Šimek, J., Houser, J., & Hritz, J. (2022). Phosphorylated and Phosphomimicking Variants May Differ—A Case Study of 14-3-3 Protein. *Frontiers in Chemistry*, *10*. https://doi.org/10.3389/fchem.2022.835733

Li, Z., Wu, X. N., Jacquot, A., Chaput, V., Adamo, M., Neuhäuser, B., Straub, T., Lejay, L., & Schulze, W. X. (2024). Phosphoregulation in the N-terminus of NRT2.1 affects nitrate uptake by controlling the interaction of NRT2.1 with NAR2.1 and kinase HPCAL1 in Arabidopsis. *Journal of Experimental Botany*, *75*(7), 2127–2142. https://doi.org/10.1093/jxb/erad490

Lorenz, T. C. (2012). Polymerase chain reaction: Basic protocol plus troubleshooting and optimization strategies. *Journal of Visualized Experiments*, *63*. https://doi.org/10.3791/3998

Murashige, T., & Skoog, F. (1962). A Revised Medium for Rapid Growth and Bio Assays with Tobacco Tissue Cultures. *Physiologia Plantarum*, *15*, 473–497.

Narasimhan, M., Johnson, A., Prizak, R., Kaufmann, W. A., Tan, S., Casillas-Pérez, B., & Friml, J. (2020). Evolutionarily unique mechanistic framework of clathrin-mediated endocytosis in plants. *ELife*, *9*. https://doi.org/10.7554/eLife.52067

Park, Y. J., Lee, H. J., Gil, K. E., Kim, J. Y., Lee, J. H., Lee, H., Cho, H. T., Vu, L. D., Smet, I. De, & Park, C. M. (2019). Developmental programming of thermonastic leaf movement. *Plant Physiology*, *180*(2), 1185–1197. https://doi.org/10.1104/pp.19.00139

Promega. (2016). *ReliaPrep™ RNA Tissue Miniprep System Instructions for Use of Products Z6110, Z6111 and Z6112*. Promega corporation. www.promega.com

Promega. (2023). *Wizard(R) Genomic DNA Purification Kit Technical Manual #TM050*. www.promega.com

Scheepens, J. F., Deng, Y., & Bossdorf, O. (2018). Phenotypic plasticity in response to temperature fluctuations is genetically variable, and relates to climatic variability of origin, in Arabidopsis thaliana. *AoB PLANTS*, *10*(4). https://doi.org/10.1093/aobpla/ply043

Schindelin, J., Arganda-Carreras, I., Frise, E., Kaynig, V., Longair, M., Pietzsch, T., Preibisch, S., Rueden, C., Saalfeld, S., Schmid, B., Tinevez, J. Y., White, D. J., Hartenstein, V., Eliceiri, K., Tomancak, P., & Cardona, A. (2012). Fiji: An open-source platform for biological-image analysis. *Nature Methods*, *9*(7), 676–682. https://doi.org/10.1038/nmeth.2019

Tan, J., Zhou, Z., Feng, H., Xing, J., Niu, Y., & Deng, Z. (2021). Data-independent acquisition-based proteome and phosphoproteome profiling reveals early protein phosphorylation and dephosphorylation events in arabidopsis seedlings upon cold exposure. *International Journal of Molecular Sciences*, *22*(23). https://doi.org/10.3390/ijms222312856

Van Damme, D., Coutuer, S., De Rycke, R., Bouget, F. Y., Inzé, D., & Geelen, D. (2006). Somatic cytokinesis and pollen maturation in Arabidopsis depend on TPLATE, which has domains similar to coat proteins. *Plant Cell*, *18*(12), 3502–3518. https://doi.org/10.1105/tpc.106.040923

Vu, L. D., Gevaert, K., & De Smet, I. (2019a). Feeling the Heat: Searching for Plant Thermosensors. In *Trends in Plant Science* (Vol. 24, Issue 3, pp. 210–219). Elsevier Ltd. https://doi.org/10.1016/j.tplants.2018.11.004

Vu, L. D., Xu, X., Gevaert, K., & de Smet, I. (2019b). Developmental plasticity at high temperature. In *Plant Physiology* (Vol. 181, Issue 2, pp. 399–411). American Society of Plant Biologists. https://doi.org/10.1104/pp.19.00652

Vu, L. D., Xu, X., Zhu, T., Pan, L., van Zanten, M., de Jong, D., Wang, Y., Vanremoortele, T., Locke, A. M., van de Cotte, B., De Winne, N., Stes, E., Russinova, E., De Jaeger, G., Van Damme, D., Uauy, C., Gevaert, K., & De Smet, I. (2021). The membrane-localized protein

kinase MAP4K4/TOT3 regulates thermomorphogenesis. *Nature Communications*, *12*(1). https://doi.org/10.1038/s41467-021-23112-0

Wang, P., Pleskot, R., Zang, J., Winkler, J., Wang, J., Yperman, K., Zhang, T., Wang, K., Gong, J., Guan, Y., Richardson, C., Duckney, P., Vandorpe, M., Mylle, E., Fiserova, J., Van Damme, D., & Hussey, P. J. (2019). Plant AtEH/Pan1 proteins drive autophagosome formation at ER-PM contact sites with actin and endocytic machinery. *Nature Communications*, *10*(1). https://doi.org/10.1038/s41467-019-12782-6

Yperman, K., Papageorgiou, A. C., Merceron, R., De Munck, S., Bloch, Y., Eeckhout, D., Jiang, Q., Tack, P., Grigoryan, R., Evangelidis, T., Van Leene, J., Vincze, L., Vandenabeele, P., Vanhaecke, F., Potocký, M., De Jaeger, G., Savvides, S. N., Tripsianes, K., Pleskot, R., & Van Damme, D. (2021a). Distinct EH domains of the endocytic TPLATE complex confer lipid and protein binding. *Nature Communications*, *12*(1). https://doi.org/10.1038/s41467-021-23314-6

Yperman, K., Wang, J., Eeckhout, D., Winkler, J., Vu, L. D., Vandorpe, M., Grones, P., Mylle, E., Kraus, M., Merceron, R., Nolf, J., Mor, E., de Bruyn, P., Loris, R., Potocký, M., Savvides, S. N., de Rybel, B., de Jaeger, G., van Damme, D., & Pleskot, R. (2021b). Molecular architecture of the endocytic TPLATE complex. *Science Advances*, *7*(9). https://doi.org/10.1126/sciadv.abe7999

SUPPLEMENTAL FIGURES

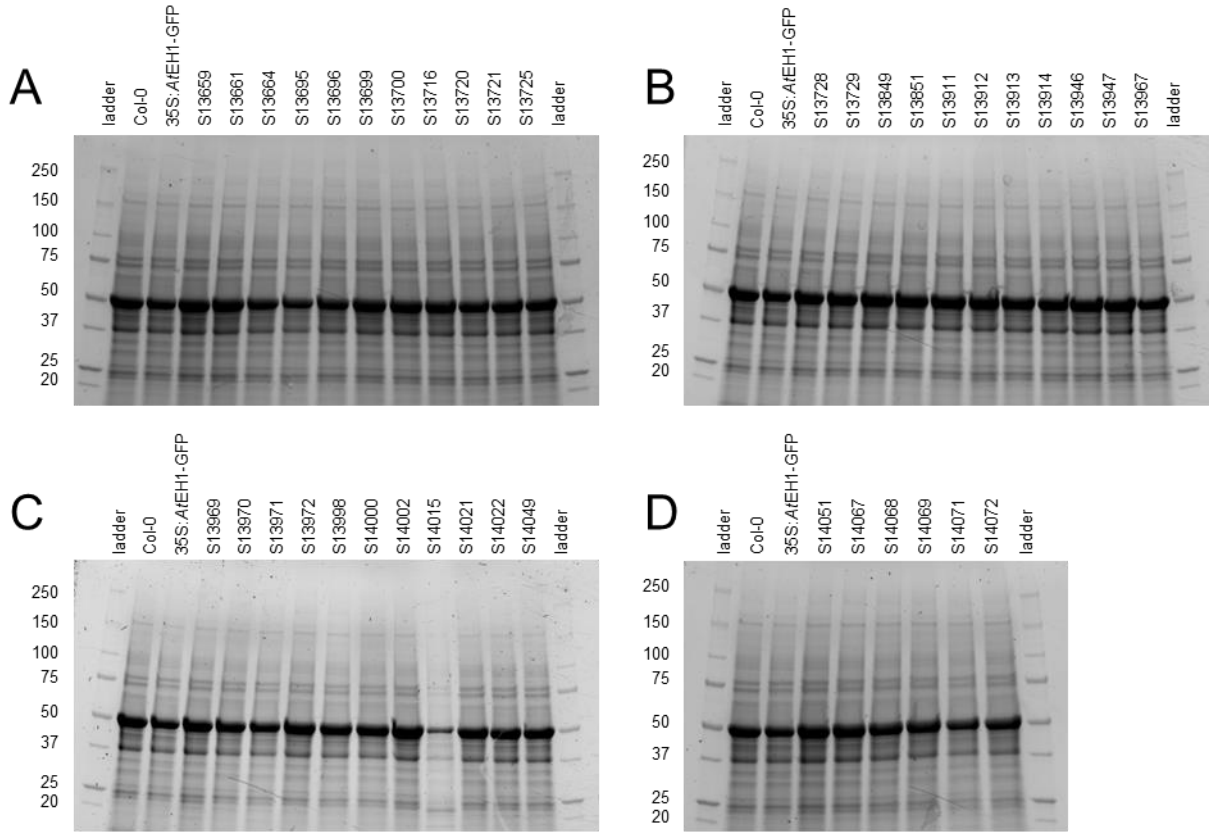

Supplemental Figure 1 In stain load controls corresponding to Figure 1. In stain load control corresponding to Figure 1A (A), in stain load control corresponding to Figure 1C (B), in stain load control corresponding to Figure 1E (C), in stain load control corresponding to Figure 1G (D).

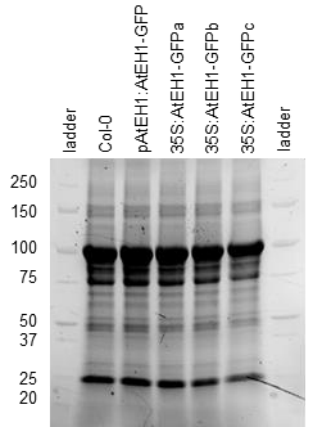

Supplemental Figure 2 In stain load control corresponding to Figure 3B.

APPLICATIONS OF THE PROJECT

This project aimed to perform fundamental research towards the phosphorylation of *At*EH1 in *Arabidopsis thaliana*, a model organism in plant research. The goal of the project was to search for a link between endocytosis and temperature-mediated phenotypic responses of plants such as leaf hyponasty and root elongation. In the light of climate change, this research could help us understand the mechanisms behind temperature response better and thus help us to improve plants to utilise these mechanisms. As I have seen in my experiments, there are indications towards a link between phosphorylated *At*EH1 and temperature-dependent phenotypic effects such as leaf hyponasty. Therefore, it is interesting to go further on these phosphorylation to use this for applications in the field. For the applications, there are two approaches possible: a genetically modified organism (GMO) and a non-GMO approach.

First for the GMO approach, I hypothesised in this project that adding phospho-mimicking sites to the protein does not have the same functionality as an actual phosphorylated protein, thus incorporating a mutated gene into the crops of interest would not have an effect on the heat resilience. But it is interesting for researchers to search for the kinase or multiple kinases causing the phosphorylation of the *At*EH proteins and their homologs in crops. If these kinases are found and their activity is researched, there is the possibility to create a more active form of these kinases in crops. This could potentially lead to more or faster phosphorylation of the homolog of the *At*EH1 protein in the crop of interest. Thus, the crop could withstand high ambient temperatures a bit better. Another possibility in the GMO-based approach would be the use of mutagenesis to downregulate the transcription or translation in the process from EH1 gene to mRNA to protein. I have seen in the experiments that overexpression of *At*EH abolishes the leaf hyponasty phenotype, this is a negative effect in the battle towards heat tolerance. Downregulation of the amount of protein expressed in the cell through downregulation of transcription or translation could assist in a better response to high ambient temperatures. Using this approach, a few things should be kept in mind, such as GMOs are not allowed everywhere in the world, there are a few countries with legislations allowing GMOs. Also

these legislations are mostly limited to a few crops, thus the use of the GMO approach would only be applicable in those countries in certain crops.

Second, the non-GMO approach or the breeding based approach. Here breeders come into play, they can look for naturally occurring plants that carry a more active kinase or that have lower expression levels of the EH1 protein. If these plants can be found in nature, the breeder can use these in combination with cultivars of interest to make crosses to create a new cultivar. This has the advantage of being permitted in all countries worldwide. A limitation of this approach would be the natural variation available.

While both strategies are promising to translate this fundamental research into an application in the field, further research is required before we could even look into these possibilities.

SUMMARY PAGE

This research investigates the interplay between phosphorylated *At*EH1, a component of the TPLATE complex which plays a role in clathrin-mediated endocytosis (CME), and temperature-mediated hyponasty. Overexpression and complementation lines were used to investigate the effect of phospho-dead and phospho-mimicking residues at ten sites in the C-terminal end of the *At*EH1 protein.

Previous research showed that overexpression lines of *At*EH1 do not lift up their leaves under stress of a higher temperature, while wild-type plants do. Therefore, I now tested phospho-mutant overexpression lines to see if there is a difference in phenotype between phospho-dead and phospho-mimicking mutants. My results showed that both phospho-mutants abolish the phenotype of the overexpression line of the endogenous gene. This indicates that one or multiple of the sites included in these mutants influence the phenotype. I also hypothesised based on my research and research described in literature that the phospho-mimicry doesn’t have the same functionality as actual phosphorylation. Therefore, further research using phospho-dead mutants each with one less mutated site may provide insight into which site is responsible for the phenotypic effect.

On the other hand, I was curious to see if disabling the phosphorylation switch would have a detrimental effect on the protein and on plants at temperatures of 28 °C. For this part of the experiments, i used *eh1-1*(+/-) plants to insert the same mutant genes as tested in the overexpression lines. If the construct is functional, it is possible to generate *eh1-1*(-/-) complementation lines. These complementation lines were then used in a root growth assay in which seedlings were grown at 21 °C and at 28 °C to compare the root growth between the two. The measurements taken at 28 °C were normalised with the results at 21 °C. After the normalisation, a statistical test was performed which showed no significant difference between the Col-0 control line and the complementation lines tested. I concluded that there is no functional impairment of the phospho-mutated *At*EH1 protein at 28 °C. Further research is necessary to investigate the functionality of the phosphorylation switch defective mutants in more detail.

In conclusion, this work provides valuable insights into the role of *At*EH1 in temperature-mediated responses and lays the groundwork for future research into the specific sites of phosphorylation that influence phenotypic effects.